AD-A171 475   INVESTIGATION OF THE EARLY TIME RESONANCE REGION   1/2
           SCATTERING PROBLEM(U) GENERAL RESEARCH CORP SANTA
           BARBARA CA ADVANCED TECHNOLOGIES D.. J R AUTON ET AL.
UNCLASSIFIED   JUN 86 GRC-CR-86-1053 N00014-84-C-0663   F/G 17/9   NL

CROCOPY RESOLUTION TEST CHART
NATIONAL BUREAU OF STANDARDS-1963-A

CR-86-1053

Investigation of the Early Time Resonance Region Scattering Problem

Final Report

by
J.R. Auton
M.L. VanBlaricum

June 1986

ADVANCED TECHNOLOGIES DIVISION

GENERAL
RESEARCH CORPORATION

P.O. BOX 6770, SANTA BARBARA, CALIFORNIA 93160-6770

DTIC
ELECTE
SEP 0 2 1986
D
E

AD-A171 475

DTIC FILE COPY

86 9 2 095

REPORT DOCUMENTATION PAGE

1a. REPORT SECURITY CLASSIFICATION UNCLASSIFIED	1b. RESTRICTIVE MARKINGS
2a. SECURITY CLASSIFICATION AUTHORITY	3. DISTRIBUTION / AVAILABILITY OF REPORT
2b. DECLASSIFICATION / DOWNGRADING SCHEDULE	UNCLASSIFIED/UNLIMITED

4. PERFORMING ORGANIZATION REPORT NUMBER(S) CR-86-1053	5. MONITORING ORGANIZATION REPORT NUMBER(S)

6a. NAME OF PERFORMING ORGANIZATION GENERAL RESEARCH CORPORATION	6b. OFFICE SYMBOL (If applicable)	7a. NAME OF MONITORING ORGANIZATION OFFICE OF NAVAL RESEARCH ELECTRONICS DIVISION, CODE 414
6c. ADDRESS (City, State, and ZIP Code) P.O. BOX 6770 SANTA BARBARA, CA 93160-6770		7b. ADDRESS (City, State, and ZIP Code) 800 NORTH QUINCY STREET ARLINGTON, VIRGINIA 22217-5000

8a. NAME OF FUNDING / SPONSORING ORGANIZATION Same as 7a	8b. OFFICE SYMBOL (If applicable)	9. PROCUREMENT INSTRUMENT IDENTIFICATION NUMBER N00014-84-C-0663

8c. ADDRESS (City, State, and ZIP Code) Same as 7b	10. SOURCE OF FUNDING NUMBERS			
	PROGRAM ELEMENT NO.	PROJECT NO.	TASK NO.	WORK UNIT ACCESSION NO.

11. TITLE (Include Security Classification)

INVESTIGATION OF THE EARLY TIME RESONANCE REGION SCATTERING PROBLEM

12. PERSONAL AUTHOR(S)
J.R. AUTON, M.L. VAN BLARICUM

13a. TYPE OF REPORT FINAL	13b. TIME COVERED FROM 9/1/84 TO 4/30/86	14. DATE OF REPORT (Year, Month, Day) 1986, June, 25	15. PAGE COUNT 96

16. SUPPLEMENTARY NOTATION

17. COSATI CODES			18. SUBJECT TERMS (Continue on reverse if necessary and identify by block number)
FIELD	GROUP	SUB-GROUP	SINGULARITY EXPANSION, SEM, FORCED RESPONSE, ENTIRE FUNCTION, SCATTERING, TARGET IDENTIFICATION RADAR CROSS SECTION, RCS

19. ABSTRACT (Continue on reverse if necessary and identify by block number)

SEE REPORT

20. DISTRIBUTION / AVAILABILITY OF ABSTRACT ☐ UNCLASSIFIED/UNLIMITED ☐ SAME AS RPT ☐ DTIC USERS	21. ABSTRACT SECURITY CLASSIFICATION SEE REPORT
22a. NAME OF RESPONSIBLE INDIVIDUAL	22b. TELEPHONE (Include Area Code) 22c. OFFICE SYMBOL

DD FORM 1473, 84 MAR 83 APR edition may be used until exhausted. All other editions are obsolete.

SECURITY CLASSIFICATION OF THIS PAGE

INVESTIGATION OF THE EARLY TIME
RESONANCE REGION SCATTERING PROBLEM

FINAL REPORT

Jon R. Auton

M.L. VanBlaricum

Submitted to:
Office of Naval Research
Electronics Division, Code 414
800 North Quincy Street
Arlington, Virginia 22217-5000
Attention: Dr. Michael A. Morgan
Final Report for Contract No. N00014-84-C-0663

DTIC
COPY
INSPECTED
1

June 1986

Accession For
NTIS
DTIC
Unan
Justi

By
Distribution/
Availability Codes
Avail and/or
Dist   Special

A-1

ABSTRACT

In addition to the pole series in the singularity expansion of a scatterer's response a "possible entire function" contribution has been customarily included although considerable uncertainty surrounds the role of this response component. Entire functions are frequently found in the responses of circuits where they represent forced components. The results of this investigation indicate that in certain extreme system configurations, like circuits, the forced response to a time-limited excitation is an entire function. In certain less extreme configurations, like most scatterers, the forced response takes the form of a "quasi-entire function" which is composed of highly-damped pole contributions. We demonstate that true entire functions themselves can be represented by infinite pole series whose poles have become infinitely-damped. For many scatterers two groups of poles can be distinguished: the dominant poles and the highly-damped poles whose contributions comprise a quasi-entire function. The numerically-derived quasi-entire function components of a conducting sphere-capped cylinder and a conducting loop are determined by subtracting the dominant pole series from the total responses of these scatterers. These results indicate that the forced response of scatterers, i.e., the quasi-entire function, may find concise description in a form similar to extended physical optics, wherein the shadowing effects inherent in the standard definition of physical optics are ignored.

ACKNOWLEDGMENTS

CONTENTS

ILLUSTRATIONS

ILLUSTRATIONS (Cont.)

ILLUSTRATIONS (Concl.)

1   INTRODUCTION

Over the years since the invention of the singularity expansion method (SEM),[1] there has been some uncertainty surrounding the identity and role of the "possible entire function" term in the singularity expansion of a scatterer's response. The fact that the entire function does not have a unique definition causes the role of this component to be somewhat vague. The results presented herein represent an attempt to grasp the meaning and utility of the entire function. The present investigation seeks to answer the following questions: (1) Is an entire function component required for the accurate representation of transient scattering responses? (2) What is the physical significance of an entire function component? (3) For applications such as resonance estimation and radar target identification, how can an entire function component be represented, dealt with, or effectively used?

Entire functions are frequently found in the frequency-domain responses of circuits where they represent forced components in the responses. Forced components are distinguished from the unforced or natural responses of a system in that they exist only while the system is under excitation, whereas the unforced response may exist independently of the excitation. Although the unforced response can exist independently, in all practical situations it is the result of some past (or present) excitation. Therefore, the label "unforced" is misleading. In fact, the forced response can be thought of as that part of the total response which quickly damps out after the excitation is removed and the unforced response is the remainder with little real distinction between the two components. The recognition of this similarity between the forced and unforced components is crucial for understanding one facet of the entire function's role in transient scattering.

As is shown in Sec. 2 for the far-field response of a conducting sphere under plane wave illumination, an entire function component is not required. On the other hand, if the sphere is deformed through the

prolate spheroids into an infinitely thin filament, an entire function is required. As the poles of the sphere are tracked from the sphere to the filament, some of the poles approach the imaginary axis in the s-plane while the rest tend to $s = -\infty$. The poles that withdraw to infinity give rise to an entire function whicn can be thought of as the forced component of the filament's response. In the time-domain, this forced component is a square-pulse function, i.e., a time-limited func- tion, that is non-zero only while the incident plane wave is on the scatterer.

In Sec. 3, the approximation of time-limited functions with sums of highly damped exponentials is found to be theoretically feasible although in practice such approximation encounters numerical difficul- ties. In the frequency-domain, this type of approximation corresponds to representing an entire function by a pole series involving poles with large negative real parts. The practical difficulties inherent with such a representation points out the effectiveness of the entire func- tion as an approximation. For distributed systems, the entire function component can be used as an approximate representation for the contribu- tion of an infinitely large group of poles that recede to infinity in the complex frequency plane. The forced components in the responses of circuits are, in fact, based on such approximations. In an absolute sense, an entire function may never be required in the responses of real systems. In a practical sense, however, the entire function can provide a welcome refuge from all the numerical problems posed by attempting to represent transient responses by pole series with infinite numbers of terms.

Such practical considerations motivate the present investigation. Radar target identification has been suggested as a possible application of the SEM representation wherein the poles of a radar scatterer are used to identify it. Poles are particularly useful features for target identification because they are invariant with aspect angle. The

authors first became acquainted with the question of the entire function
while estimating resonances from measurements of transient scattering
from thin cylinders. We noticed that only when the early-time portions
of the back scattered returns were excluded from the resonance estima-
tion procedure (Prony's method) could consistent estimates of the reson-
ances be achieved. At the time, we speculated that the early-time data
was not composed purely of the unforced response, but also included a
forced component which could not be adequately modeled by the finite
pole series being matched to the data. The results of the present in-
vestigation confirm this initial speculation.

Because an infinite number of degrees of freedom exist in the
residues of a scatterer's pole series, there is considerable freedom in
the choice of the entire function. The residues can, in many cases, be
adjusted to absorb or produce an additional arbitrary entire function in
the representation. In Sec. 3, it is shown that the Laplace transform
of a time-limited function can be represented to any degree of accuracy
by a pole series formed from poles with large negative real parts.
Since most scatterers possess an infinite number of such poles, any
entire function resulting from an arbitrary time-limited function in the
early-time response can be expanded in those poles to any degree of
accuracy. As a result, there is usually a variety of choices for entire
function and one simply has to make a good choice.

Heyman and Felsen[2] have suggested that for many types of scat-
terers, such as the sphere, pole series are not very useful in the
representation of the early-time response. Instead, they suggest that,
for many scatterers, the responses can be more efficiently represented
if groups of resonances are combined into the wavefronts and rays of the
geometrical theory of diffraction for the early-time responses, while
the SEM pole series can be retained for late times if the late-time

response is significant. Wavefronts are nothing more than entire function components. Specifically for the conducting sphere, Überall and Gaunaurd[3] have shown how the scattered fields of the conducting sphere can be split into a geometrical-optics and creeping-wave components. The geometrical-optics component corresponds to an entire function and the creeping waves to a pole series in the frequency domain. Mathematically, this entire function has no meaning since it could be excluded from the representation altogether. Numerically, the inclusion of this component accelerates the convergence of the representation. Physically, this component can be given meaningful interpretation as the reflection from the apex of the sphere. This choice for the entire function is, of course, one among many.

Morgan[4] and Pearson[5] have suggested that the entire function is required in addition to the pole series to accurately describe the scatterer's response. The results of the present investigation do not bear out the absolute necessity of the entire function in the responses of scatterers but only its usefulness in the accurate and efficient representation of the early-time response. Morgan's[4] entire function represents another possibly good choice for the entire function.

For many scatterers, it is possible to distinguish two groups of poles: the highly-damped poles and the dominant poles. The contributions of the highly-damped poles can be grouped into what we will call a "quasi-entire function" component. In Sec. 4, the quasi-entire components of two scatterers, a conducting cylinder and loop, are numerically derived by subtracting the dominant pole series from the total responses. Both class 1 and class 2 coupling coefficients are used to form the pole series which results in two definitions of the quasi-entire function for each case, thus illustrating the non-uniqueness of this response component. The quasi-entire function may be regarded as a forced response component in the same spirit as the forced responses of circuits. As the results of Sec. 4 illustrate, this forced component resembles the extended physical optics[4,6] response of the scatterer.

2   EXAMPLES AND COUNTEREXAMPLES OF REQUIRED ENTIRE FUNCTION COMPO-
NENTS IN TRANSIENT RESPONSES

To illustrate the basic issues under consideration, some simple
systems that can be analyzed by exact methods allow some preliminary
conclusions to be made. First, a circuit shown in Fig. 2.1, whose
transfer function contains both an entire function component and a reso-
nant component is considered. The transfer function of this circuit can
be written as
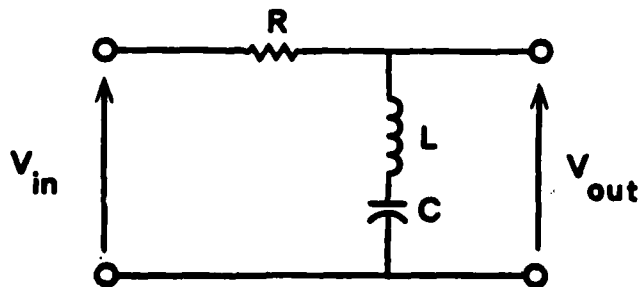
$$H(s) = \frac{V_{in}(s)}{V_{out}(s)} = 1 + A_1(s - s_1)^{-1} + A_2(s - s_2)^{-1} \qquad (2.1)$$

where

$$s_{1,2} = -\frac{R}{2L} \pm j\left[\frac{1}{LC} - \left(\frac{R}{2L}\right)^2\right]^{1/2}$$

$$A_1 = -\frac{R}{L}\frac{s_1}{s_1 - s_2}$$

$$A_2 = -\frac{R}{L}\frac{s_2}{s_2 - s_1}$$

AN-75842

Figure 2.1. A network whose transfer function contains an entire
function and a pole series.

with $1/(LC) \geq R^2/(2L)^2$. The first term of Eq. 2.1 is a (constant) entire function of the Laplace transform variable $s = \sigma + j\omega$. The presence of this term causes the output of the circuit to contain the familiar forced component. The remaining two terms comprise a finite pole series that constitutes the unforced or natural response of the circuit. The entire function in this case is required for the accurate representation of the response.

Next, consider the direct connection between input and output formed by replacing the R element of Fig. 2.1 by a short and the L and C elements with an open. The transfer function of this network is $H(s) = 1$ and the response consists only of a forced entire-function component. This direct connection can be thought of as transmission line observed at low frequencies. At high frequencies, a transmission line of length L with a voltage generator, V_{in} , at the input and an open at the output as shown in Fig. 2.2 has a transfer function given by

$$H(s) = \frac{1}{\cos(-jsL/c)} \tag{2.2}$$

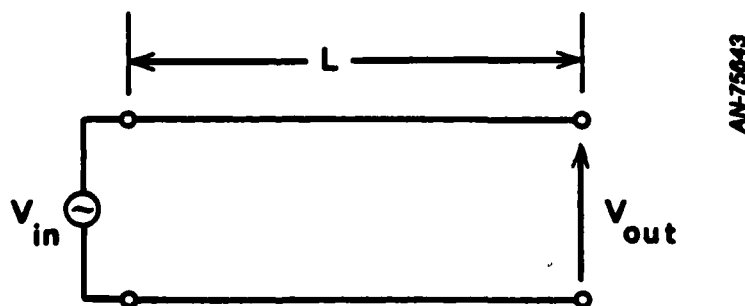where c is the speed of light. The transfer function has poles,

Figure 2.2. A transmission line as a network whose transfer function can be represented exactly as an infinite pole series alone or approximately at low frequencies by an entire function alone.

$$s_n = j \frac{(2n + 1)c\pi}{2L} \qquad n = 0, \pm 1, \pm 2, \ldots$$

and can be expanded into a pure pole series with an infinite number of
terms. Note that at low frequencies Eq. 2.2 can be approximated as
$H(s) = 1$. It then becomes obvious that the entire function found in
circuit theory is a result of the low frequency approximations that form
the basis of circuit theory. A large number of high frequency resonant
contributions can be combined and approximately represented as an entire
function accurately within limited region of the complex-frequency
plane.

The above considerations indicate that an entire function contri-
bution may never exist in reality but is merely a convenient approximate
representation for a large number of high-frequency resonant contribu-
tions. The question to answer then becomes: how is the entire function
to be defined in specific cases? The answer to this question appears to
be that no precise or unique definition is ever possible. However, in
certain extreme system configurations, the system poles will frequently
cluster into widely separated regions of the complex plane. In such
cases, the definition of the entire function can take on a measure of
precision and uniqueness. One such extreme configuration is the infi-
nitely thin wire scatterer which is explored below. Other such config-
urations are circuits of which an example has already been given. Next,
we will consider two scatterer geometries, namely the sphere and the
infinitely thin wire, which illustrate the extremes with regard to the
entire function question.

The conducting sphere is one scatterer that can be solved entirely
by analytical techniques. Moreover, the poles of the sphere are found
by finding the zeros of polynomials, as is done for circuits, instead of
more complicated functions as is the case for most, if not all other
scatterers. The scattered far field of a perfectly conducting sphere in

free space with an +x-polarized incident plane wave traveling in the +z direction can be written as[1,7-9]

$$\overline{E}^s = - j \frac{\exp(-jkR)}{R} \sum_{n=1}^{\infty} \frac{2n + 1}{n(n + 1)}$$

$$\times \left\{ \frac{j_n(ka)}{kh_n^{(2)}(ka)} \left[\frac{P_n^1(\cos \theta)}{\sin \theta} \cos \phi \hat{\theta} - \frac{dP_n^1(\cos \theta)}{d\theta} \sin \phi \hat{\phi} \right] \right.$$

$$\left. + \frac{[kaj_n(ka)]'}{k[kah_n^{(2)}(ka)]'} \left[\frac{dP_n^1(\cos \theta)}{d\theta} \cos \phi \hat{\theta} - \frac{P_n^1(\cos \theta)}{\sin \theta} \sin \phi \hat{\phi} \right] \right\} \qquad (2.3)$$

where P_n^1 is the associated Legendre function of the first kind of order 1 and degree n, j_n and $h_n^{(2)}$ are spherical Bessel functions of the first and third kinds, respectively, a is the radius of the sphere, $k = \omega/c = -js/c$ is the wave number, and R is the distance to the far field point. The deriviatives of the spherical Bessel functions appearing in Eq. 2.3 are defined by

$$[kaz_n(ka)]' = \frac{d}{dx} [xz_n(x)] \Big|_{x=ka} = z_{n-1}(ka) - \frac{n}{ka} z_n(ka)$$

where z_n denotes the Bessel function. Equation 2.3 can be converted into a pole series plus an entire function by expanding the factors

$$\frac{j_n(ka)}{kh_n^{(2)}(ka)} = \frac{1}{2k} \left[1 + \frac{h_n^{(1)}(ka)}{h_n^{(2)}(ka)} \right] \qquad (2.4a)$$

and

$$\frac{[kaj_n(ka)]'}{k[kah_n^{(2)}(ka)]'} = \frac{1}{2k}\left[1 + \frac{[kah_n^{(1)}(ka)]'}{[kah_n^{(2)}(ka)]'}\right] \qquad (2.4b)$$

into pole series and entire function terms where the spherical Bessel functions are defined by

$$h_n^{(1)}(z) = j^{-n-1}\frac{\exp(jz)}{z}\sum_{i=0}^{n}a_i(-2jz)^{-i}$$

$$h_n^{(2)}(z) = j^{n+1}\frac{\exp(-jz)}{z}\sum_{i=0}^{n}a_i(2jz)^{-i}$$

and

$$a_i = \frac{(n+i)!}{i!(n-i)!}$$

For each n, Eqs. 2.4a and 2.4b can be expanded into a pole series plus the entire function, $[1 - \exp(j2ka)]/(2k)$. These entire functions can be summed over n to give a total entire function component in the sphere's response. Upon examination, this component displays some rather peculiar features, has no apparent physical interpretation, and is regarded as a mathematical artifact.

Although when each of the factors in Eq. 2.4 are taken individually, an entire function term must exist for each term of Eq. 2.3; this does not indicate that the total response requires an entire function. In Sec. 3, it is shown that the residues of a pole series with a large number of deeply-imbedded poles can always be adjusted to absorb the entire function into the pole series. Since the sphere possesses such a set of poles, the response of the sphere should be representable to any

degree of accuracy by a pole series alone. It is always possible, though, to rearrange the equations so that an entire function component is retained. In this case, the residues of the resulting pole series are altered to account for the additional component.

Next the infinitely thin conducting wire or filament scatterer is considered. This scatterer requires an entire function component, in addition to a constant coefficient pole series, to accurately represent its scattered field and thus it provides a counter example to that of the sphere. Finally, the transition from sphere through the prolate spheroids to the filament will be explored and there the specific causes of the difference between the sphere and the filament with regard to the entire function will become clear.

To develop a solution for the axial currents on a filament with a plane wave incident field, we start with an asymptotic solution obtained for an infinitely long conducting cylinder driven by voltage across an infinitely thin gap, given by Chen and Keller.[10] This solution, which is valid for large $k|z - z'|$, can be written as an admittance which, when multiplied by the gap voltage, gives the current:

$$\tilde{Y}^\infty(z,z',s) \approx \frac{2\pi}{\eta} \frac{\exp(-s|z - z'|/c)}{\log(2j|z - z'|/a) - \log(-j\Gamma^2 sa/c)} \qquad (2.5)$$

where $\eta = \sqrt{\mu_o/\epsilon_o}$ is the impedance of free space in which the cylinder is immersed, a is the radius of the cylinder, $\Gamma \approx 1.781$ is the exponential of Euler's constant, z' is the z coordinate of the gap and z is the coordinate for the location of the current. The tilde denotes a Laplace transformed quantity.

For very small ka , Eq. 2.5 can be written in a simpler form:

$$\tilde{Y}^\infty(z,z',s) \approx Y_o \exp(-s|z - z'|/c) \qquad (2.6)$$

2-6

where

$$Y_o = - \frac{2\pi}{\eta \, \log \, \omega_o a/c} \; ,$$

and ω_o is a constant such that $\omega_o \simeq \omega$. In transient analysis, ω will vary over some range. In this case, ω_o is set to the middle of this range.

Equation 2.6 is valid even for $k|z - z'| \ll 1$ when ka is very small. However, in a region very close to the gap, Eq. 2.6 does not adequately account for the logarithmic singularity in the current. Near the gap, the current is given by[10]

$$\tilde{Y}^\infty \simeq - \frac{4jka}{\eta} \, \log \, k|z - z'|$$

As $ka \to 0$, this component has a vanishingly small effect compared to the other components of current given by Eq. 2.6 and, hence, it can be neglected.

The solutions of Eqs. 2.5 and 2.6 assume that a gap, i.e., an opening in the metal, exists, and that the gap voltage has no variation in ϕ so that no ϕ-directed currents are excited on the cylinder. Some resolvable differences then exist between the gapless filament under excitation by an arbitrary plane wave and the cylinder. The gap in the cylinder can be closed without any change in the exterior fields. This is done by defining fields of the gap-excited cylinder as scattered fields, closing the gap with a perfect conductor, and introducing an incident field to cancel with the electric field corresponding to the gap voltage on the perfect conductor. It will be assumed that the ϕ components of the incident plane wave electric field on the cylinder's surface and the ϕ-directed currents produced by these components have negligible effects on the overall response of the filament. This is a

standard thin-wire assumption which is known to produce correct results as ka approaches zero. The φ-variation of the incident field obviously becomes negligible as ka approaches zero.

Applying the inverse Laplace transform to Eq. 2.6 gives the time domain form:

$$Y^{\infty}(z,z',t) \approx Y_o \delta(t - |z - z'|/c) \tag{2.7}$$

where $\delta(t)$ is the Dirac delta function. Equation 2.7 approaches the exact solution away from the gap for the time-domain current on an infinitely long filament excited locally at z' by a delta function incidence field. Equation 2.7 represents two current impulses traveling in both directions away from the excitation point.

Equation 2.7 can be used to determine the currents on a filament of finite length. The reflections of the current pulses off the ends of a finite filament can be modeled with additional sources (infinitely thin gaps with voltages across them) situated at the ends and defined such that the currents at the ends are always zero. Chen and Keller[10] give a detailed description of the modeling of the ends of the cylinder. The time-domain current on a filament of length L excited by a localized E-field or voltage source at z' can then be written as

$$Y(z,z',t) = Y_o \sum_{n=0}^{\infty} \left\{ \delta(ct - z + z' - 2nL) + \delta(ct + z - z' - 2nL) \right.$$

$$- \delta[ct - z - z' - (2n + 1)L]$$

$$\left. - \delta[ct + z + z' - (2n + 1)L] \right\} u(t) \tag{2.8}$$

where u(t) is the unit step function. Equation 2.8 represents the two current impulses traveling away from z' and recurrently reflecting off the ends of the finite filament.

Filament currents due to an incident impulsive plane wave, as shown in Fig. 2.3, can be found by superposition, using

$$I(z,t) = E_z^i \int_{-L/2}^{L/2} Y(z,z',t + z' \cos \theta') \, dz' \qquad (2.9)$$

where E_z^i is the z component of the incident electric field. Similarly, the scattered far field can be found from

$$E_\theta(\theta,t) = \frac{\mu \sin \theta}{4\pi R} \frac{\partial}{\partial t} \int_{-L/2}^{L/2} I(z,t + z \cos \theta - R) \, dz \qquad (2.10)$$

where θ is the scattering angle and R is the distance to the far field. The currents and fields given by Eqs. 2.9 and 2.10 are composed of the superposition of a number of step functions in time.
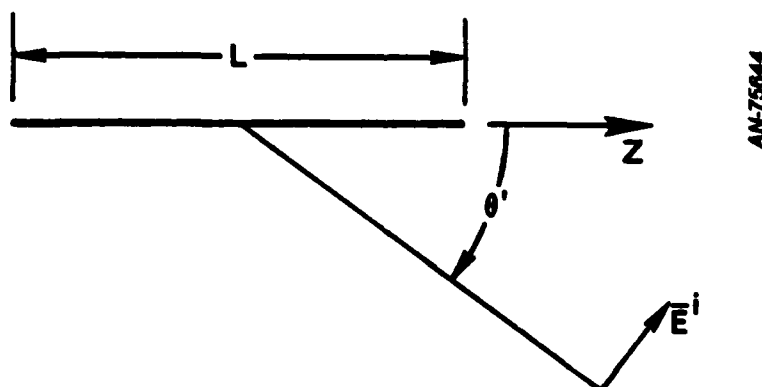
Figure 2.3. Geometry for scattering by filament scatterer of length L.

Figure 2.4 illustrates the time history of the backscattered far field produced by an infinitely thin filament of length L with impulsive plane wave excitation as found using Eq. 2.10. In Fig. 2.4, the responses of a perfectly conducting sphere-capped cylinder with a length-to-diameter ratio of 30 are provided for comparison to those of the filament. The cylinders response's were obtained using a moment-method solution of the electric field integral equation. Note that all of the features, except for the damping and amplitudes, of the filament's and cylinder's responses agree well. The late-time portions of the filament responses are completely periodic, whereas in the early-time an aperiodicity is noted. The periodic late-time portion of the response can be expanded in a Fourier series which is nothing more than the pole series employing the dominant filament resonances. However, this series cannot model the aperiodicities in the early-time portions of the filament responses. If the periodic late-time response is continued into the early-time and subtracted from the total response in the early-time, the residual is a time-limited function whose Laplace transform is an entire function.

In contrast to the sphere, a filament scatterer requires an entire function component in its far field response to plane wave excitation. What is the difference between the two cases? As is shown below, some of the sphere's poles withdraw to $s = -\infty$ as the sphere is deformed through prolate spheroids toward the infinitely thin filament. It is these large frequency poles whose contributions may be approximated quite closely by an entire function in the manner discussed above. In the limit as $ka \to 0$, the approximation becomes exact.

Figures 2.5 and 2.6 show selected pole loci for the prolate spheroid as it varies from the sphere to the filament scatterer. The geometry of the prolate spheroid is indicated in Fig. 2.7. In cylindrical coordinates, the equation for the spheroid is $\rho^2/a^2 + z^2/b^2 = 1$. The results for $b/a < \infty$ were obtained with BRFD[11] which is a scattering
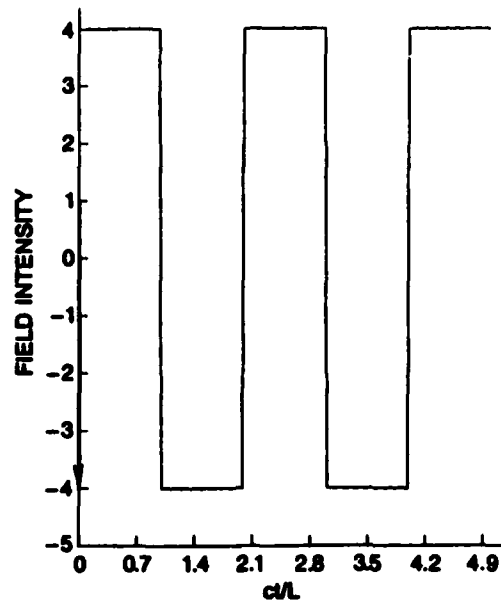
(a) Filament scatterer, $\theta = 90°$
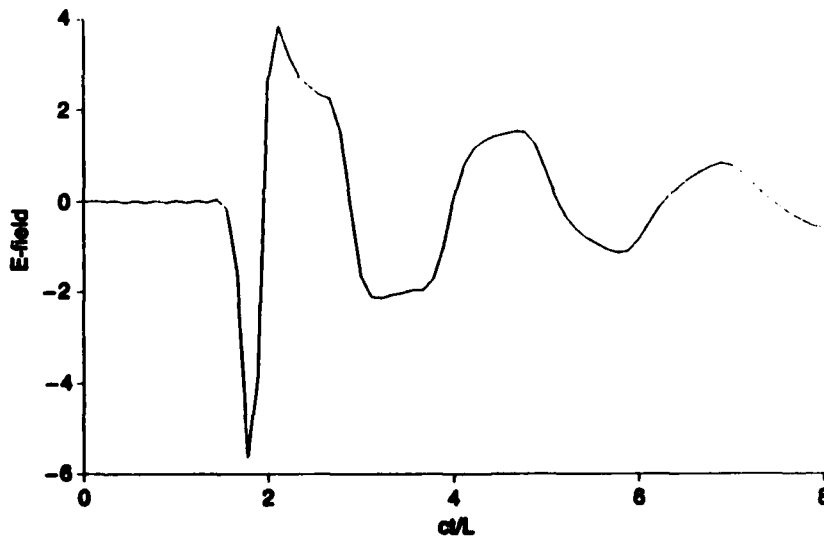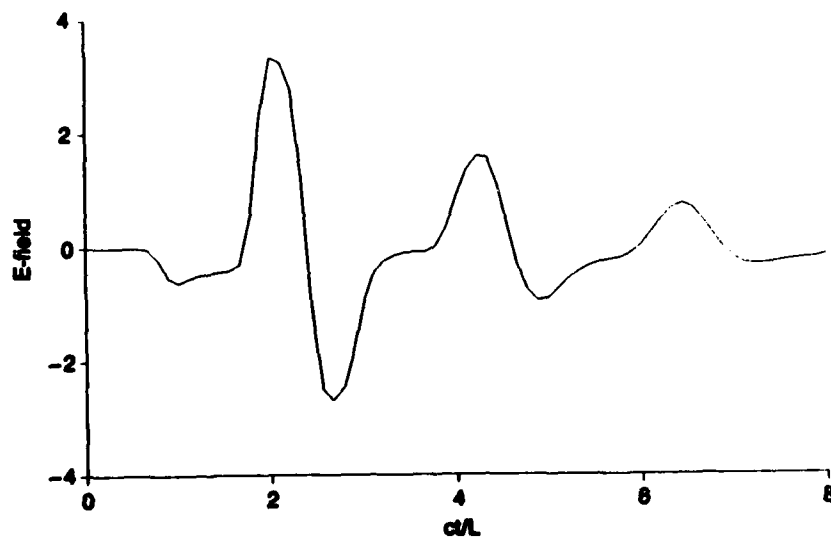

(b) Sphere-capped cylinder with a length-to-diameter ratio of 30
    ($L/D = 30$), $\theta = 90°$

Figure 2.4.   Time history of backscattered far fields due to impulsive
              plane wave excitation.
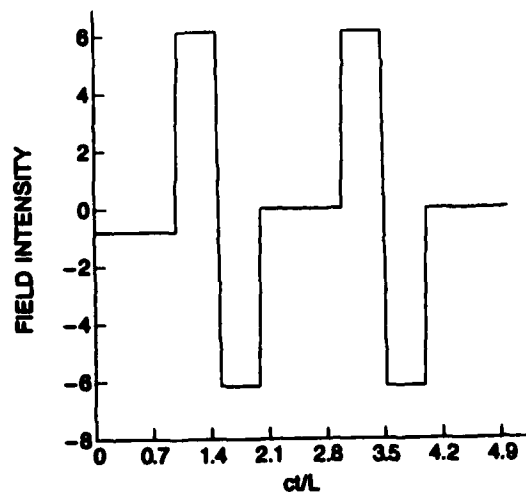
(c) Filament scatterer θ = 60°
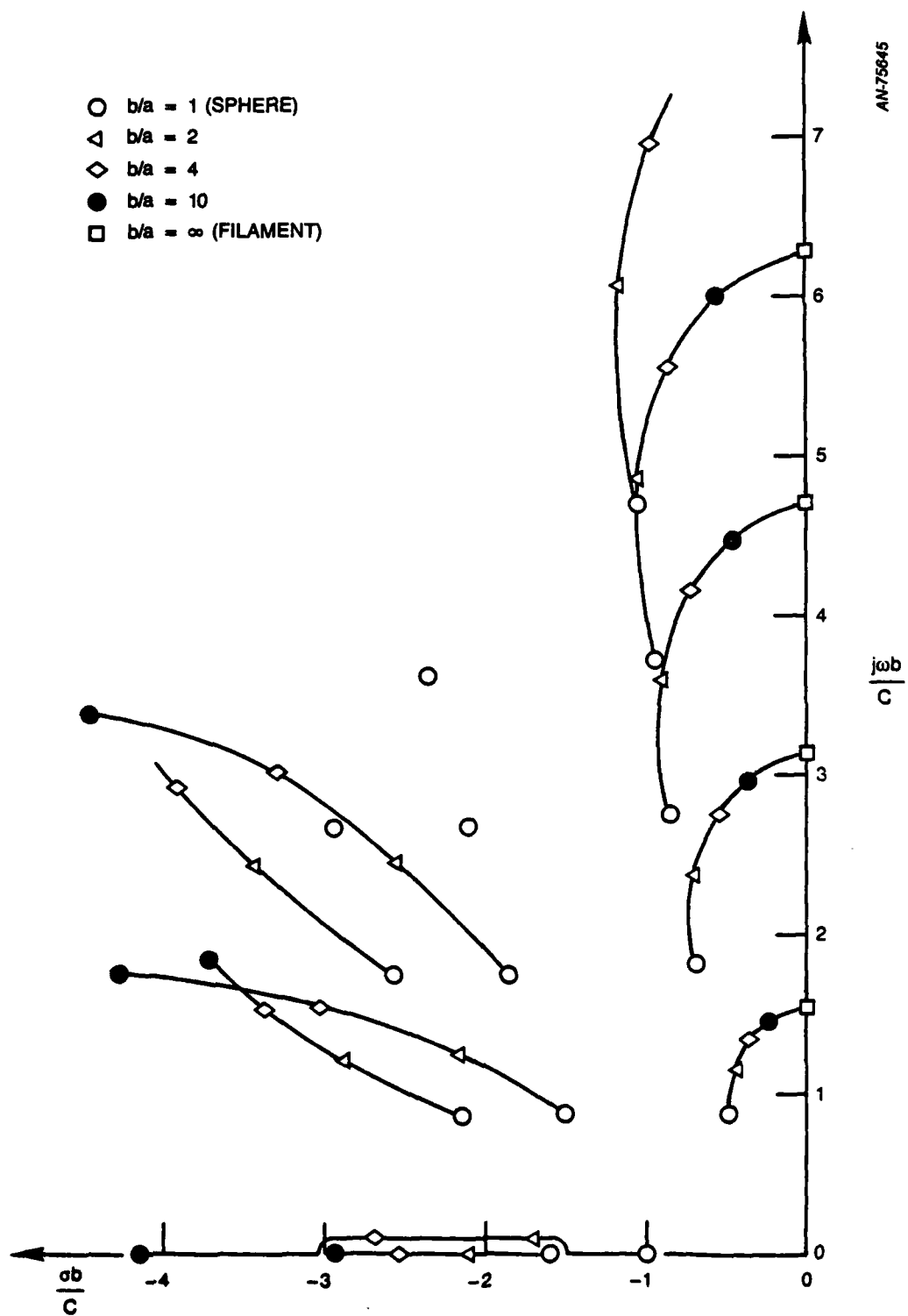
(d) Sphere-capped cylinder (L/D = 30), θ = 60°

Figure 2.4 (Cont.)

2-12

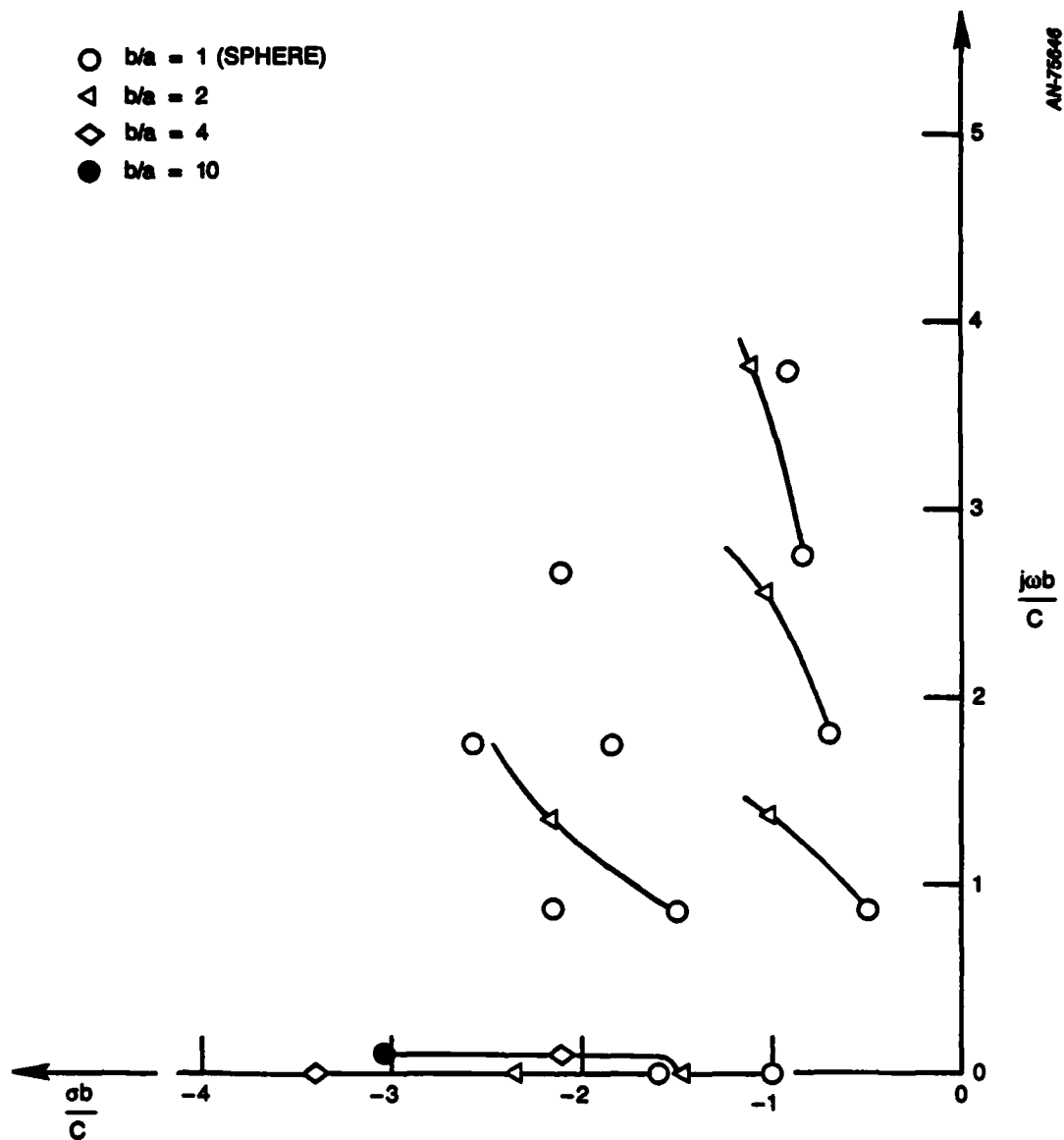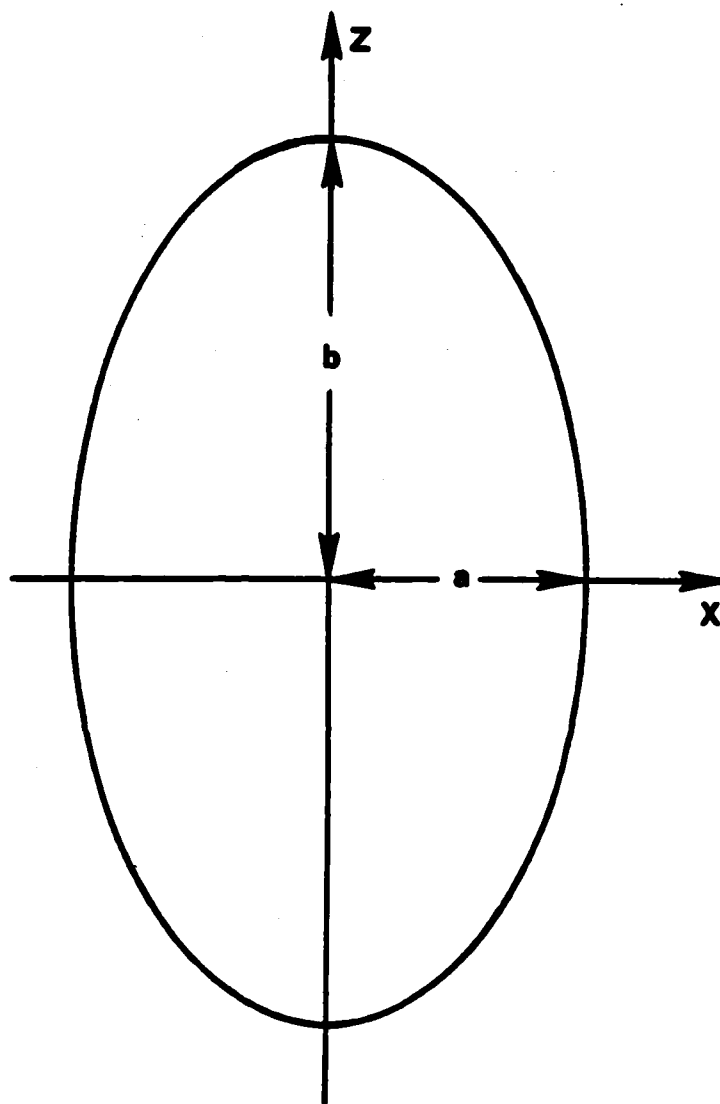Figure 2.5. Prolate spheroid pole loci for surface currents modes which are constant in φ.

2–13

Figure 2.6. Prolate spheroid pole loci for surface currents modes
which have first harmonic variation in ϕ, i.e., the
modes vary as $\exp(\pm j\phi)$.

Figure 2.7.   Geometry of prolate spheroid.

code for general conducting bodies of revolution and is based on a method-of-moments solution of the frequency-domain electric field integral equation. These results indicate that certain poles of the sphere, namely those poles in the layer nearest the imaginary axis which are associated with current modes that are constant in ϕ , migrate to the imaginary axis in the s-plane as the sphere is deformed continuously through the prolate spheroids to arrive finally at the filament scatterer. All other poles withdraw to $s = -\infty$. The periodic components of the filament responses shown in Fig. 2.4 must be composed of pole series of the filament which is nothing more than a Fourier series. The early-time aperiodic component must be due to those poles that have withdrawn to $s = -\infty$. Hence, the poles that flee to infinity must give rise to the entire function in the filament's frequency-domain response.

When the prolate spheroid is thin, but not infinitely thin, there exists a group of poles which are deeply-imbedded in the left half of the s-plane. These poles give rise to a quasi-entire function in the scatterer's frequency-domain response and are distinguished from the dominant poles which lie near the imaginary axis. For general scatterer geometries, it should always be possible to define a quasi-entire function whenever a set of dominant poles are clearly distinguishable from the rest. The numerically-derived quasi-entire functions of selected thin scatterers are examined in Sec. 4.

3 APPROXIMATE REPRESENTATION OF TIME-LIMITED FUNCTIONS BY EXPONENTIAL SUMS

In Sec. 2, we have seen that the contribution of a group of large frequency poles is an effectively time-limited component in a scatterer's response which corresponds to a quasi-entire function. In this section, the representation of actual time-limited functions by exponential series, which are the time-domain representatives of pole series, is considered. It is found that time-limited functions can be represented to any degree of accuracy with a exponential series by including a sufficient number of terms and that the best approximations are obtained if poles that are deeply-imbedded in the left half of the s-plane (Re s large and negative) are employed in the exponential series. The fact that the pole sets of scatterers usually include many such deeply-imbedded poles suggests that the residues of the complete pole series for the scatterer's response can always be adjusted to incorporate any time-limited, forced component that may exist.

First consider the approximation of the exponential entire function by a pole series. As is shown in Appendix A,

$$exp(z) \simeq N^N \prod_{i=1}^{N} (z_i - z)^{-1} \qquad (3.1)$$

where the following conditions hold

$$|z| \ll N \qquad (3.2a)$$

$$|z_i - N| \ll N \quad \text{for all } i \qquad (3.2b)$$

$$\frac{1}{N} \left| \sum_{i=1}^{N} (z_i - N) \right| \ll 1 \qquad (3.2c)$$

Note that Eq. 3.1 can be expanded in partial fractions to form a pole series. The z_i can have any distribution, so long as the conditions in Eqs. 3.2b and 3.2c are satisfied. Thus, in the finite complex plane, the exponential entire function can be approximated to any degree of accuracy by a pole series with a sufficient number of terms. Conditions in Eqs. 3.2b and 3.2c are roughly equivalent to the constraint that $z_i \simeq N$.

The Laplace transform,

$$F(s) = \int_a^b f(t)e^{-st}\,dt \quad , \quad 0 \le a < b$$

of the time-limited function, $f(t)$, can be approximated to any degree of accuracy by choosing M sufficiently large in the sum

$$F(s) \approx \sum_{k=1}^{M} f(t_k)\,\exp(-st_k)\Delta t \tag{3.3}$$

where

$$t_k = a + \left(k - \frac{1}{2}\right)\Delta t$$

and

$$\Delta t = (b - a)/M$$

Here we assume that $f(t)$ satisfies the usual conditions for the existence of the transform. Replacing z with $-st_k$ and z_i with $z_{ik} = -s_{ik}t_k$ in Eq. 3.1, and substituting into Eq. 3.3 gives

$$F(s) \simeq -\sum_{k=1}^{M} f(t_k) \Delta t N^N \prod_{i=1}^{N} (z_{ik} - z)^{-1} \qquad (3.4)$$

where the z_{ik} are chosen so that the conditions in Eqs. 3.2a to 3.2c are satisfied. Equation 3.4 can be expanded into partial fractions to provide a pole series for $F(s)$. Therefore, the following has been shown: The Laplace transform of any time-limited function can be approximated to any degree of accuracy over a finite region of the complex plane with a pole series. The restriction to the finite region of the complex plane is equivalent to the restriction to band-limited cases.

If Eq. 3.4 is to be a good approximation, the s_{ik} should satisfy

$$s_{ik} \simeq -N/t_k$$

for all i and k which is equivalent to saying that the poles should be deeply imbedded in the left half of the s-plane. In general, scatterers possess an infinite number of poles that satisfy this requirement.

The above observations indicate that, at least for bandlimited cases, the residues or coefficients of the pole series for a scatterer's response to an impulsive plane wave can always be adjusted to incorporate any time-limited, forced component that may exist while the incident plane wave is on the scatterer, and thus that the natural modes form a "complete" basis for the scatterer's responses. Unfortunately, this completeness property of the natural modes cannot be demonstrated with absolute rigor since the above argument is based on an assumed rough knowledge of the pole distribution in the complex frequency plane. For general scatterers, the authors' knowledge is quite limited in this regard.

To more concretely explore the question of the representation of time-limited entire functions as discussed above, the following numerical experiment was performed. A pole series of the form

$$F(s) = \sum_{i=1}^{N} A_i (i - 1)! (s + N)^i \tag{3.5}$$

which in the time domain is

$$f(t) = \sum_{i=1}^{N} A_i t^{i-1} \exp(-Nt) \tag{3.6}$$

is fit to the pulse function $u(t) - u(t - 1)$ in a least-squares sense over the interval $(0, \infty)$ by adjusting the A_i, as described in Appendix B. In Eq. 3.5, $F(s)$ has an nth order deeply-imbedded pole at $s = -N$. Figure 3.1 shows the results for $N = 2$, 4, and 6. This type of approximation on an infinite interval cannot be achieved with a Fourier series, which can only represent periodic functions, except in the limit as the Fourier series becomes the Fourier transform. The Fourier series is equivalent to a pole series whose poles are evenly spaced along the imaginary axis in the s-plane. Figure 3.1 illustrates the use of deeply-imbedded poles in a pole series for the approximation of an aperiodic, time-limited function on the infinite interval. The practicality of using such a representation, though, is questionable since as the poles move deeper into the left half of the s-plane, one encounters numerical problems. One way to avoid these problems is to abandon the pole series and resort to the entire function representation obtained by taking the Laplace transform of the pulse function. Therefore, as a practical matter, pole series using deeply-imbedded poles are abandoned in favor of other representations, one of which is the entire-function representation.
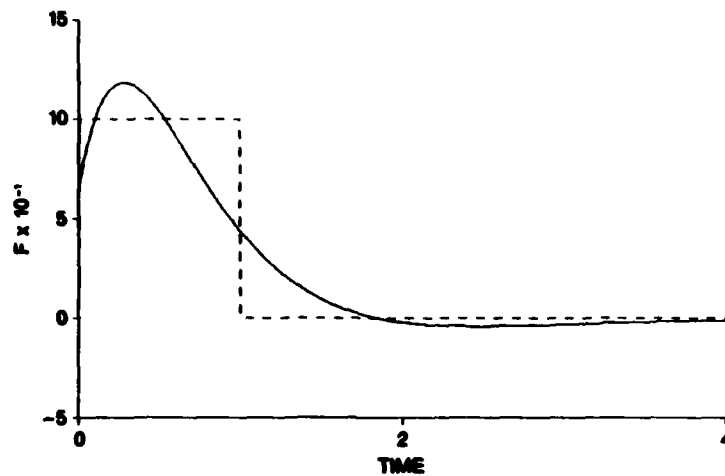
(a) Sum of 2 exponentials
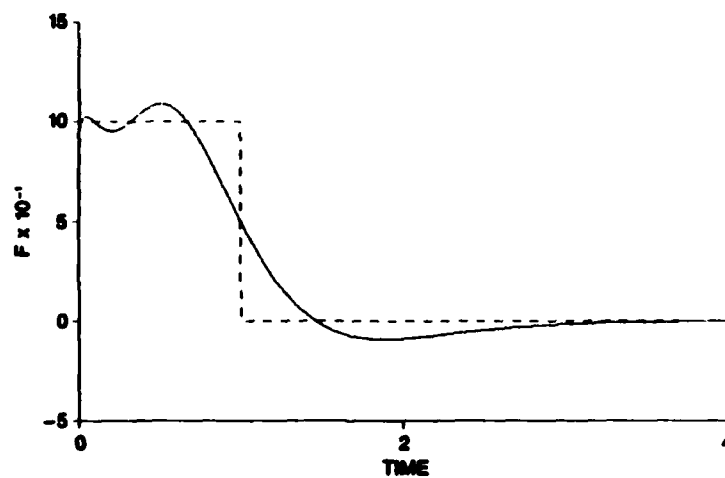
(b) Sum of 4 exponentials

Figure 3.1.   Approximation of pulse function by a sum of highly-damped
exponentials.   The dashed lines show the pulse function.
The solid lines show the approximation.
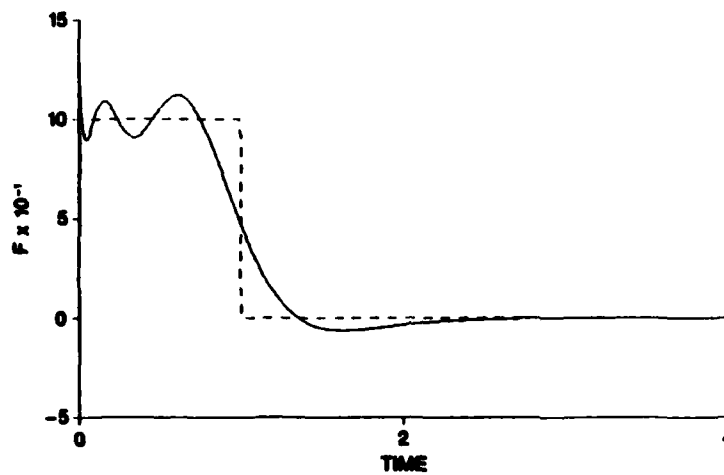
(c) Sum of 6 exponentials

Figure 3.1 (Cont.)

Ordinarily, one may resort to other representations for the quasi-entire function with impunity except while attempting to estimate the resonances with techniques like Prony's method.[12] For resonance estimation, it may be feasible to assign a number of highly-damped poles to account for the quasi-entire function in a constrained resonance estimation procedure like the constrained version of Prony's method described in Appendix C.

4   NUMERICAL EXAMPLES OF THE QUASI-ENTIRE FUNCTION

In this section, the numerically-derived quasi-entire function, which was discussed in Sec. 1, of the conducting loop (torus) and the sphere-capped cylinder are examined. Both of these scatterers possess a clearly distinguishable set of dominant resonances when they are sufficiently thin.

The method for isolating the quasi-entire function consists of subtracting the pole series constructed with the dominant poles from the total response. The pole series is constructed through use of the electric field integral equation (EFIE) for a perfectly-conducting body, which can be written as

$$\Gamma \bar{J} = \hat{n} \times \bar{E}^i \tag{4.1}$$

where $\bar{J}$ is the surface current density, $\bar{E}^i$ is the incident electric field, $\hat{n}$ is the outward-pointing unit vector normal to the scatterer's surface, and Γ is a linear operator defined by

$$\Gamma \bar{J} = \hat{n} \times \left(j\omega\mu\bar{A} + \frac{1}{j\omega\varepsilon} \nabla\phi \right)$$

The magnetic vector potential, $\bar{A}$, and electric scalar potential, ϕ, are defined as

$$\bar{A}(\bar{r}) = \int_S \bar{J}(\bar{r}\,') \frac{\exp(-jkR)}{4\pi R} \, ds'$$

$$\phi(\bar{r}) = \int_S \nabla' \cdot \bar{J}(\bar{r}\,') \frac{\exp(-jkR)}{4\pi R} \, ds'$$

where the integrals are over the scatterer's surface, S, and $R = |\bar{r} - \bar{r}'|$.

The method of moments[13] is applied to convert the EFIE into a set of matrix equations. The conversion is accomplished by first expanding the current on a set of basis functions, $\{\bar{f}_m(\bar{r}), m = 1, \ldots, M\}$, as

$$\bar{J}(\bar{r}') = \sum_m J_m \bar{f}_m(\bar{r}') \qquad (4.2)$$

Next, define an inner product

$$(\bar{f}, \bar{g}) = \int_S \bar{f} \cdot \bar{g} \; dS$$

Finally, a set of testing functions $\{\bar{g}_m, m = 1, \ldots, M\}$ is defined and a set of equations is formed by taking the inner product of Eq. 4.1 with each of the testing functions. Using Eq. 4.2, these equations can be written as

$$\sum_{m=1}^{M} J_m (\Gamma \bar{f}_m, \bar{g}_n) = (\hat{n} \times \bar{E}^i, \bar{g}_n) \qquad n = 1, 2, \ldots, M$$

These equations can be written in matrix form as

$$ZI = V$$

where the nth element of V is $(\hat{n} \times \bar{E}^i, \bar{g}_n)$, the mth element of I is J_m, and the nth-mth element of Z is $(\Gamma \bar{f}_m, \bar{g}_n)$.

Assuming only first order dominant poles, the response for the scatterer currents may be written in the form[14,15]

$$I(s) = \sum_{\alpha} (s - s_{\alpha})^{-1} v_{\alpha} \eta_{\alpha}(s) + W(s) \qquad (4.3)$$

where s_{α} are the dominant natural frequencies or poles, v_{α} are the natural mode vectors, $\eta_{\alpha}(s)$ are the coupling coefficients, and W is, as it is used here, the quasi-entire function which contains contributions from all poles not included in the dominant pole set, as well as contributions from any true entire function that may exist.

The various quantities in Eq. 4.3 can be determined in the manner described by Baum.[14,15] The poles are found by a search procedure (Newton's method) as the zeroes of the determinant of $Z = Z(s)$. That is, the poles satisfy $\det(Z_{\alpha}) = 0$ where $Z_{\alpha} = Z(s_{\alpha})$. The natural mode vectors satisfy $Z_{\alpha} v_{\alpha} = 0$. In addition, coupling vectors, u_{α}, are defined and satisfy $u_{\alpha}^T Z_{\alpha} = 0$. The coupling coefficients are found as

$$\eta_{\alpha}(s_{\alpha}) = \frac{u_{\alpha}^T V_{\alpha}}{u_{\alpha}^T Z_{\alpha}' v_{\alpha}}$$

where V_{α} is the value of V at s_{α} and

$$Z_{\alpha}' = \frac{d}{ds} Z(s) \bigg|_{s=s_{\alpha}}$$

The coupling coefficients are not uniquely defined and may assume any number of forms at frequencies away from the poles. Two forms which will be used for present purposes are the "class 1" form:[14,15]

4-3

$$\eta_\alpha^{(1)}(s) = \exp[(s_\alpha - s)t_0] \, \frac{u_\alpha^T V_\alpha}{u_\alpha^T Z'_\alpha v_\alpha}$$

where t_0 is the turn-on time of the series and the "class 2" form:

$$\eta_\alpha^{(2)}(s) = \frac{u_\alpha^T V(s)}{u_\alpha^T Z'_\alpha v_\alpha}$$

The turn-on time is chosen as the time at which the impulsive planewave first touches the scatterer.

Figures 4.1 and 4.2 show the geometries for the conducting sphere-capped cylinder and the conducting loop scatterers. Both scatterers are bodies of revolution (BORs) and results were obtained with the BRFD code[11] which uses a method-of-moments solution of the frequency-domain electric field integral equation specialized for BORs. BRFD can determine the resonant poles, modes, and coupling coefficients, as well as the current and scattered field responses. Time-domain results are obtained by inverse Fourier transforming the frequency-domain responses. The scatterer geometry is described by a generating contour which, when rotated about the z-axis, sweeps through the surface of the BOR. The surface coordinates t and ϕ are used to define locations on the BOR's surface where t is the arc length along the generating contour. Surface currents are broken into t and ϕ-directed components.

Figure 4.3 and Tables 4.1 through 4.4 define the dominant poles for the two cylinders and two loops that are used to construct a pole series which is then subtracted from the total response to find the residual response which corresponds to the quasi-entire function, as defined in Eq. 4.3. Figures 4.4 through 4.7 show both total and residual t-directed currents for the $L/D = 10$ cylinder for θ-polarized
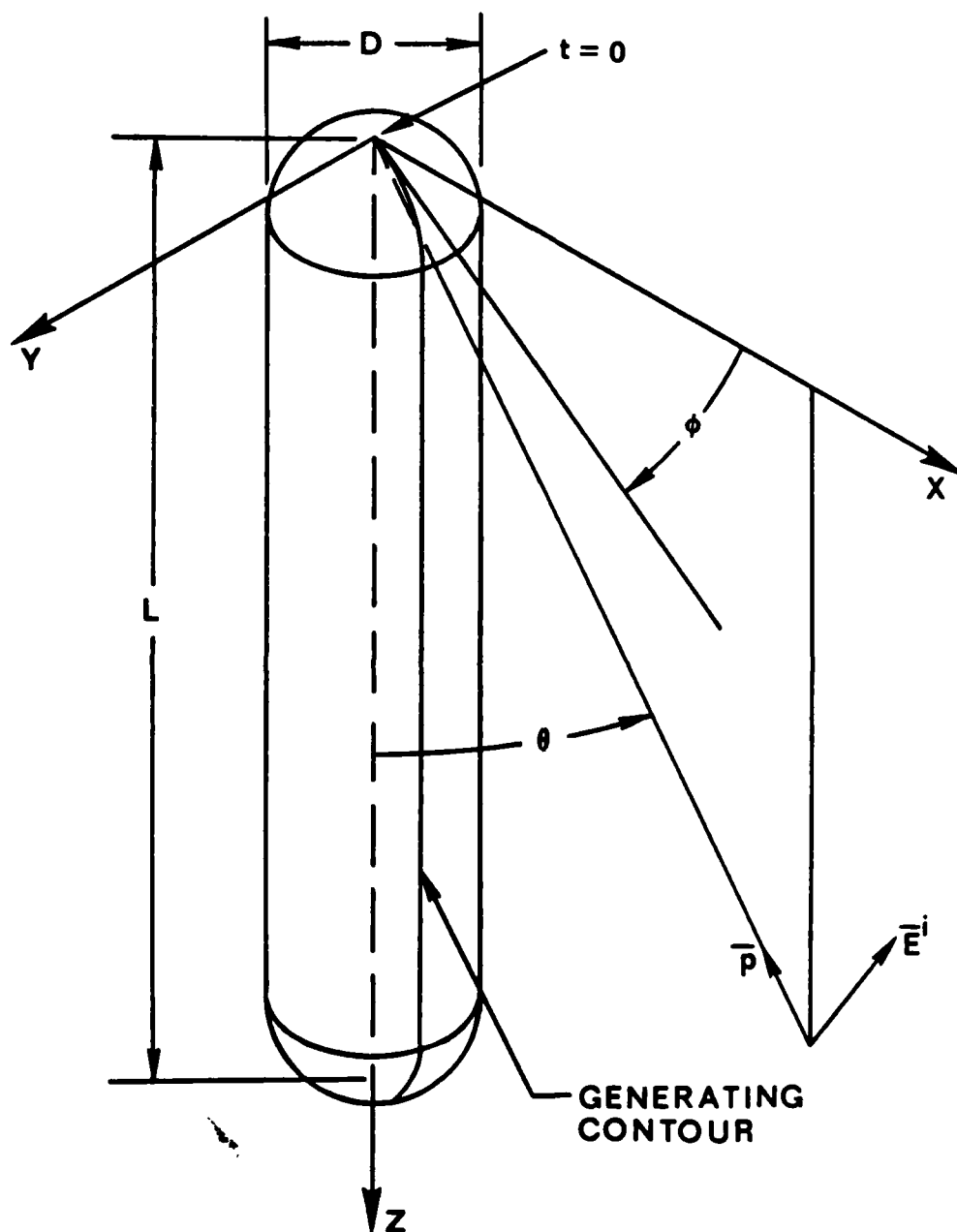
Figure 4.1. Sphere-capped cylinder geometry. Arc length along generating contour is denoted as t.
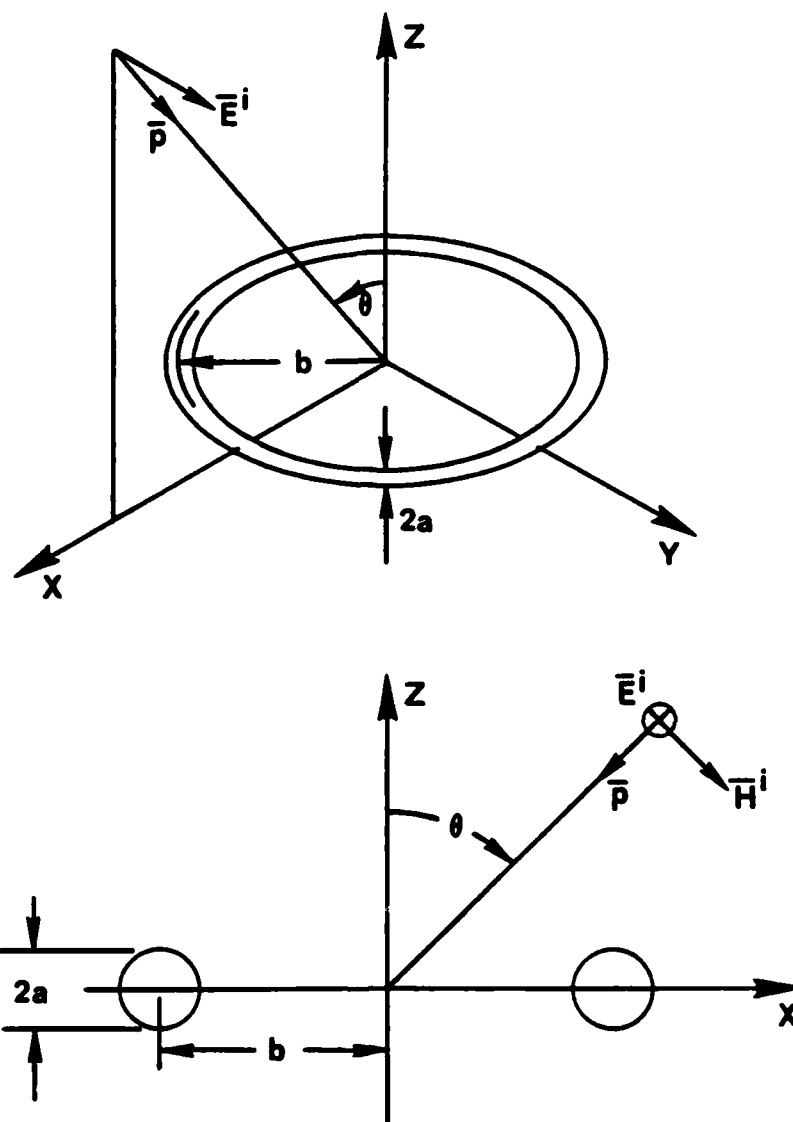
Figure 4.2. Loop (torus) geometry.
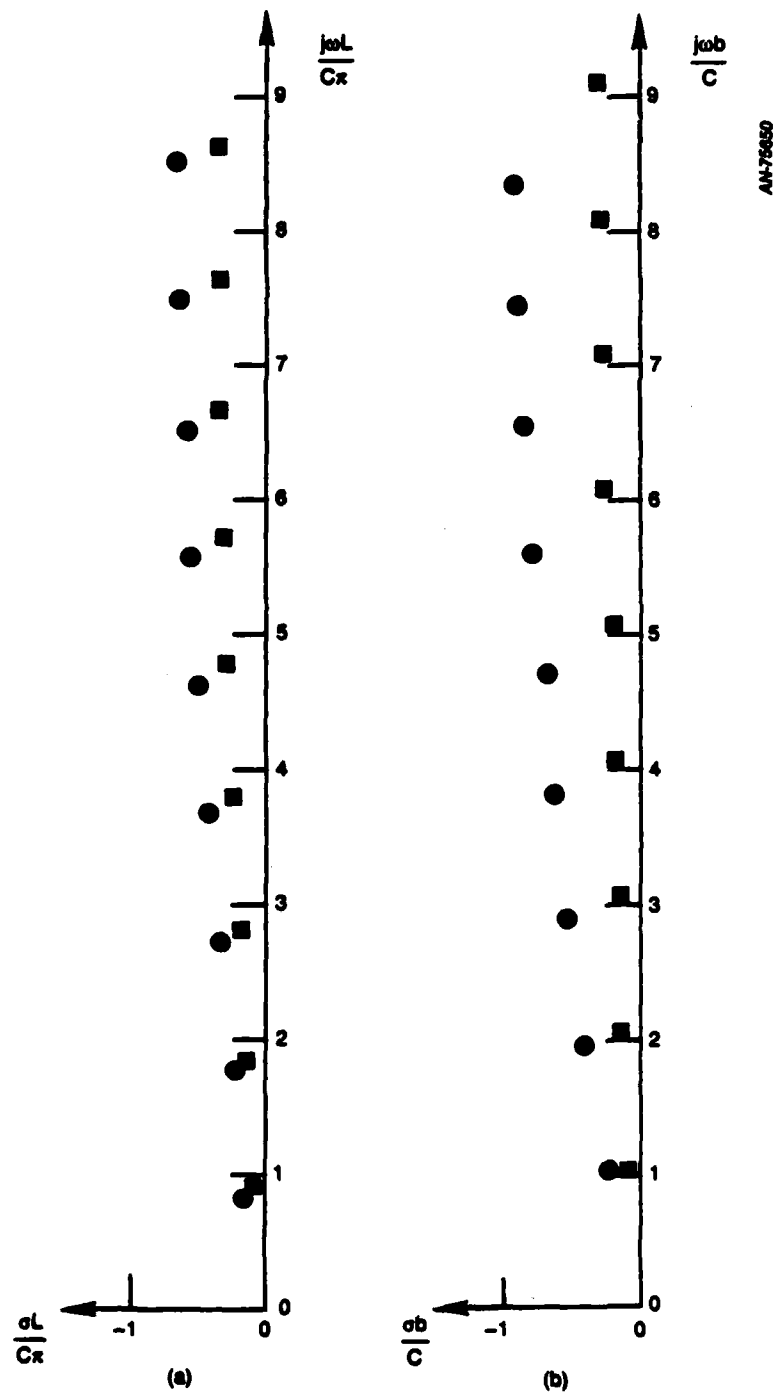
Figure 4.3. Dominant poles for (a) conducting sphere-capped cylinder with (●) L/D = 10 (■) L/D = 30, and (b) conducting loop with (●) b/a = 10 (■) b/a = 100.

Table 4.1. Poles for sphere-capped cylinder with L/D = 10.

$$s_k L/c\pi$$

k	Real	Imag
1	-0.1404751	0.822279
2	-0.2389305	1.760744
3	-0.3280972	2.721550
4	-0.4203163	3.68549
5	-0.5030614	4.627963
6	-0.5693341	5.567039
7	-0.6114042	6.515115
8	-0.6424545	7.497416
9	-0.6786275	8.528675

Table 4.2. Poles for sphere-capped cylinder with L/D = 30.

$$s_k L/c\pi$$

k	Real	Imag
1	-0.1014181	0.8725323
2	-0.1575135	1.828658
3	-0.2035508	2.803896
4	-0.2478629	3.785218
5	-0.2912341	4.760835
6	-0.3279485	5.724434
7	-0.3504116	6.681224
8	-0.3586058	7.644284
9	-0.3629002	8.620916

Table 4.3. Poles for loop with b/a = 10.

	$s_k b/c$	
k	Real	Imag
1	-0.2404304	1.034475
2	-0.3971459	1.989159
3	-0.5232771	2.913365
4	-0.6255311	3.824480
5	-0.7108793	4.730809
6	-0.7844273	5.635828
7	-0.8495169	6.541081
8	-0.9083419	7.447382
9	-0.9624029	8.355284

Table 4.4. Poles for loop with b/a = 100.

|	$s_k b/c$	
k	Real	Imag
1	-0.0958744	1.045078
2	-0.1417687	2.061150
3	-0.1777874	3.072605
4	-0.2085869	4.081876
5	-0.2358296	5.089798
6	-0.2602842	6.096767
7	-0.2823390	7.103003
8	-0.3021917	8.108644
9	-0.3199142	9.113752
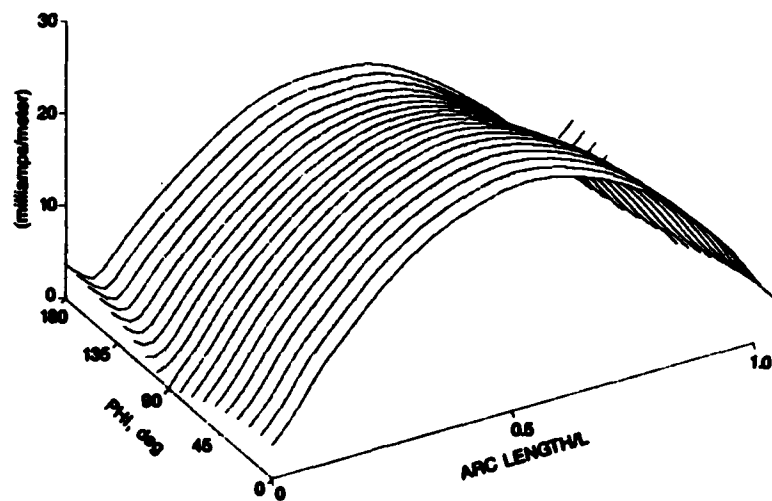
(a) Total currents
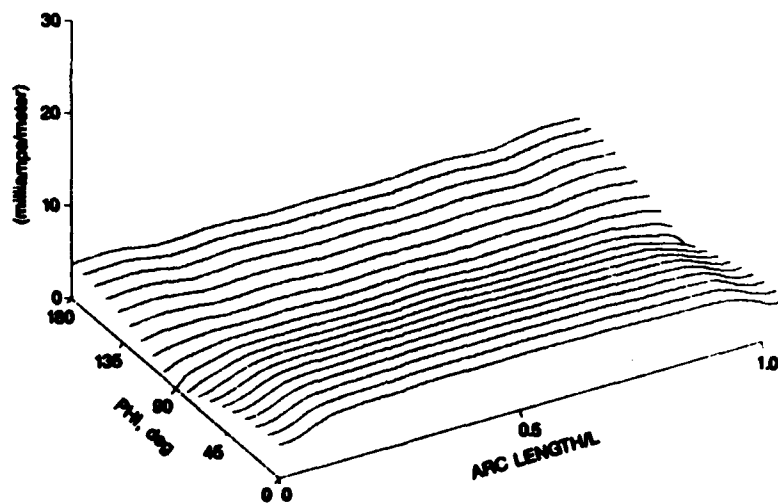
(b) Class 1 residual currents

Figure 4.4. Surface currents on sphere-capped cylinder at frequency of
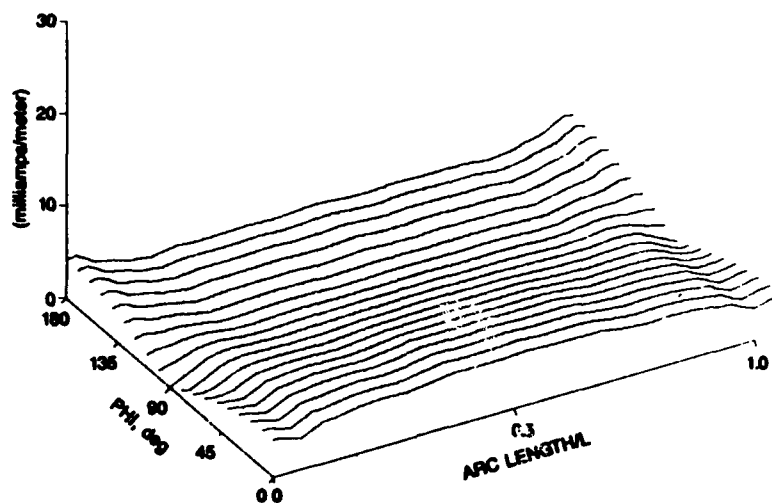c/2L and an incident angle of θ = 90 degrees.
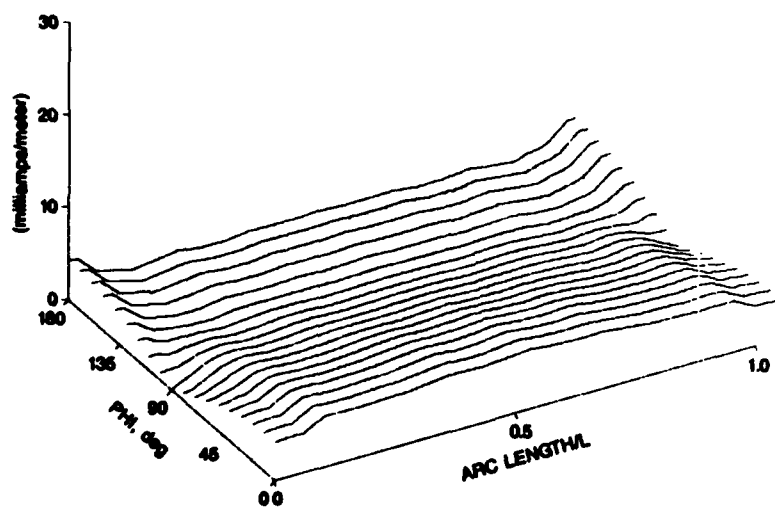
4-10
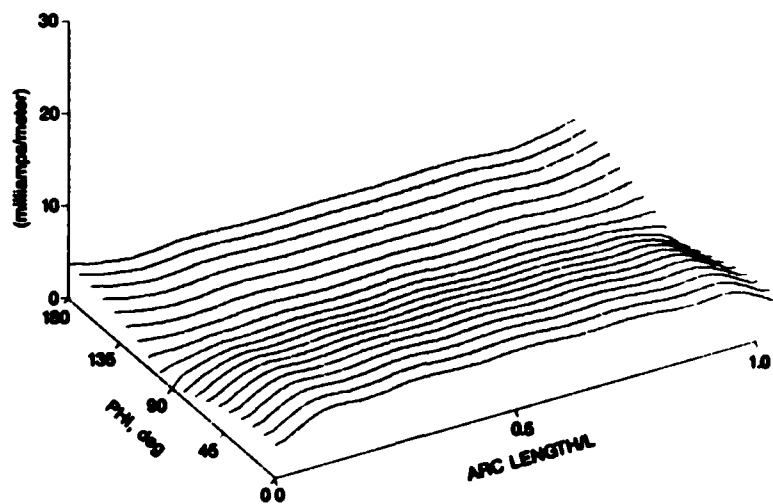
(c) Class 2 residual currents

Figure 4.4 (Cont.)
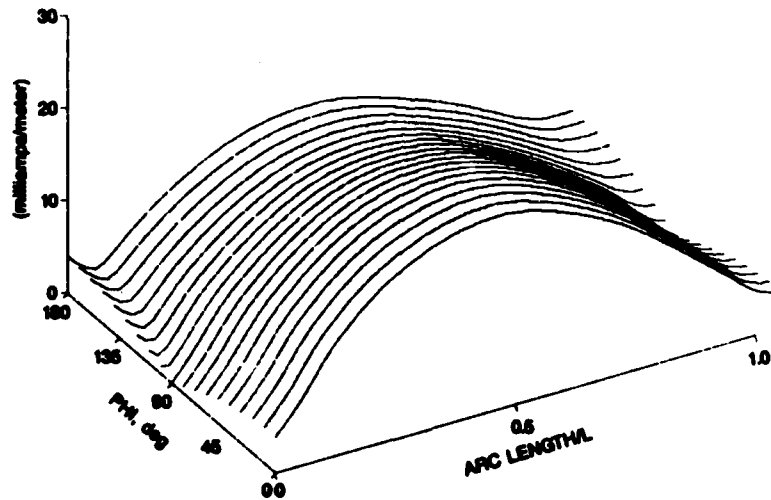
(a) Total currents

Figure 4.5. Surface currents on sphere—capped cylinder at a frequency of c/2L and an incident angle of θ = 60 degrees.

4–11
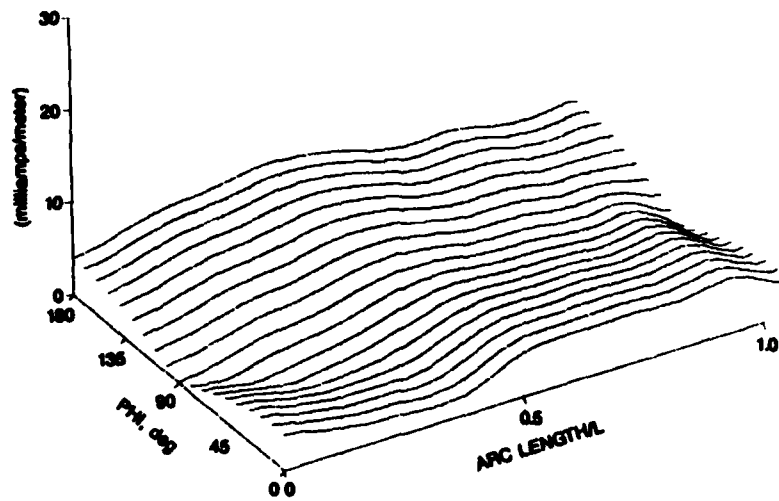
(b) Class 1 residual currents
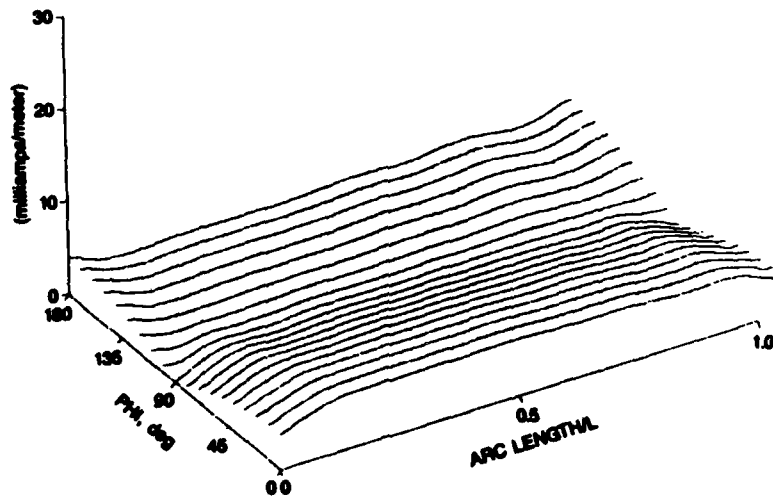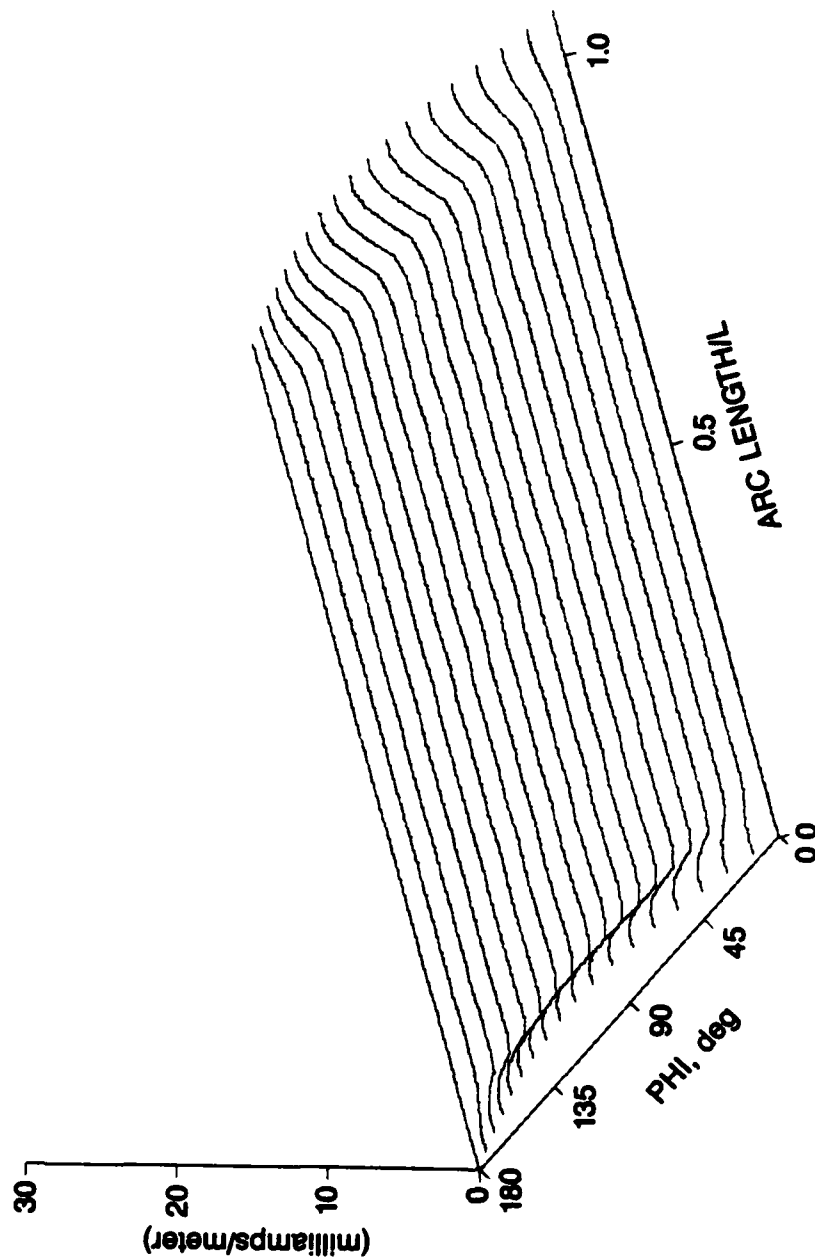

(c) Class 2 residual currents

Figure 4.5 (Cont.)
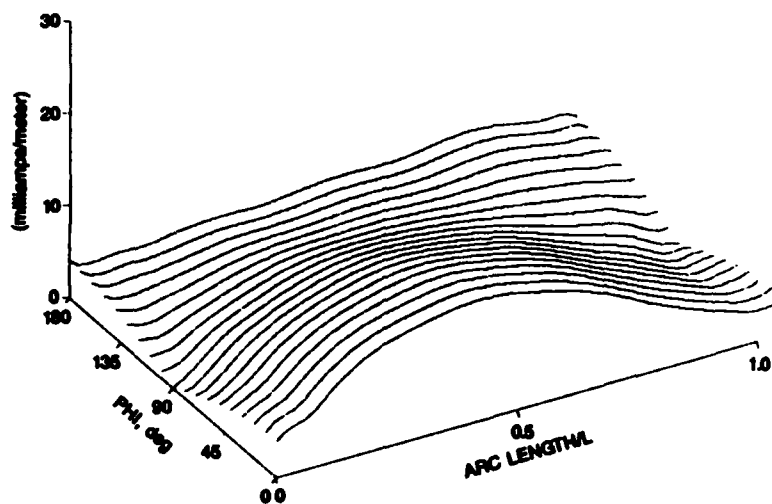
(a) Total currents
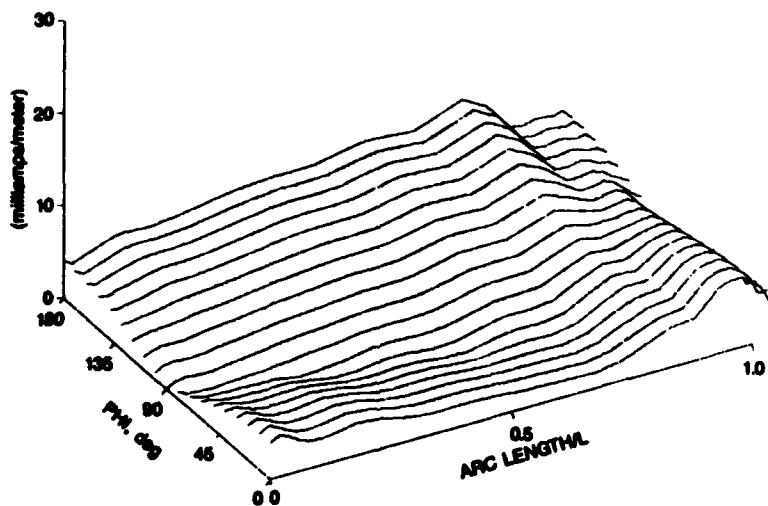
(b) Class 1 residual currents

Figure 4.6.   Surface currents on sphere–capped cylinder at a frequency
of c/2L and an incident angle of θ = 30 degrees.

4–13
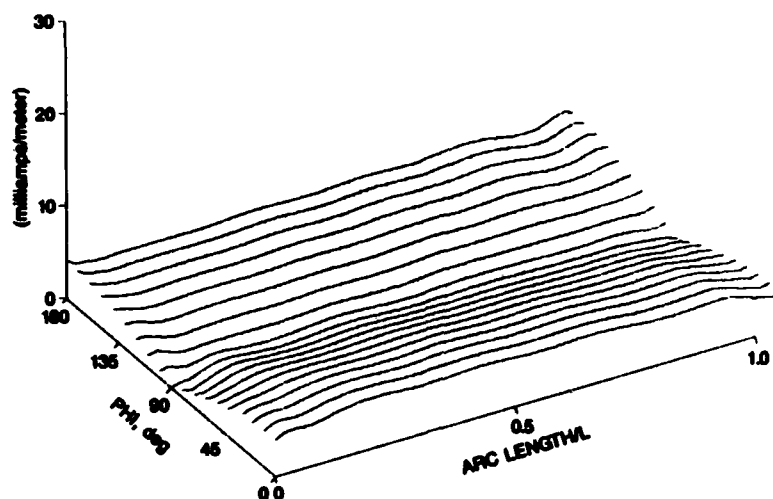
(c) Class 2 residual currents

Figure 4.6 (Cont.)
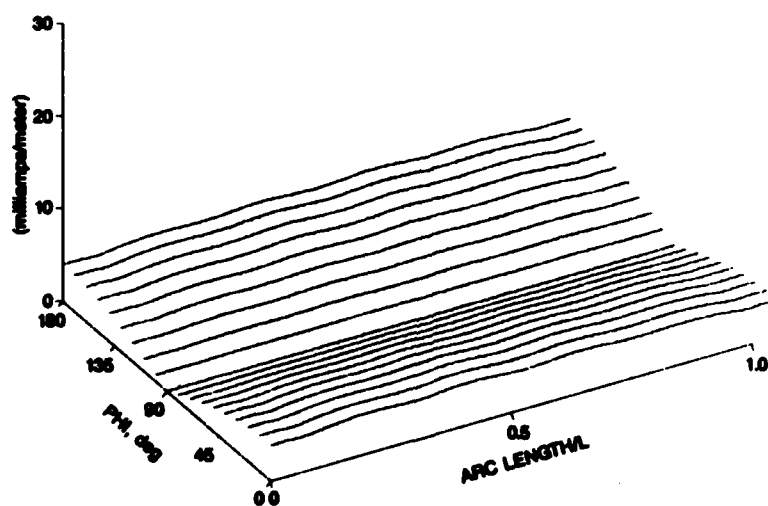
(a) Total currents

Figure 4.7. Surface currents on sphere–capped cylinder at a frequency
of c/2L and an incident angle of θ = 0 degrees.

(b) Class 1 residual currents

(c) Class 2 residual currents

Figure 4.7 (Cont.)

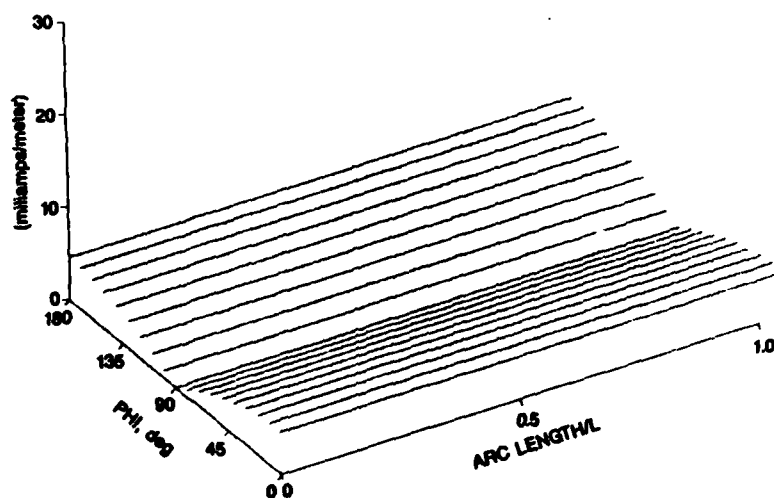incident plane wave from directions $\theta = 90, 60, 30$, and 0 degrees and $\phi = 0$ degrees at the frequency $c/2L$ (near the first resonant frequency of the cylinder). The residual currents obtained by using both class 1 and class 2 coupling coefficients are shown. The incident electric field magnitude is one volt/meter. Figures 4.8 and 4.9 show the same for frequencies 2 and 3 $c/2L$ with incident angle $\theta = 90$ degrees. Figure 4.10 shows ϕ-directed currents at the frequency $c/2L$ and an incident angle $\theta = 0$ degrees. The phi-directed currents, both total and residual, for other angles and other incident directions are almost identical in magnitude to the currents shown in Fig. 4.10. Figure 4.11 shows "extended physical optics" currents,[4,6] so called here because they ignore shadowing effects. That is, the extended physical optics currents are defined by $\bar{J} = 2\hat{n} \times \bar{H}^i$ over the entire surface of the scatterer. To be true physical optics currents, those currents between $\theta = 90$ and 180 degrees, as well as certain currents near the ends of the cylinder, should be zero. While the currents shown in Fig. 4.11 are for an incident angle of $\theta = 90°$, the magnitudes of the currents do not change with frequency or incident angle.

Several features of the currents are noteworthy. First, the magnitudes of the class 2 residual currents are almost, if not entirely, independent of both the incident angle and the frequency. Second, the residual currents show a strong resemblance to the extended physical optics currents of Fig. 4.11 and a lesser resemblance to the true physical optics currents. Third, at an incident angle of $\theta = 0$ degrees, the total and residual currents are virtually identical, that is, the dominant pole contributions appear to be minimal for this angle of incidence. The true physical optics currents contribute significantly more to the far fields than do the currents of Fig. 4.11, since the currents on the front and back sides of the cylinder tend to cancel for the latter currents. However, in spite of the resemblance between the extended physical optics and residual currents, the contributions of the residual and true physical optics currents to the far fields are comparable due
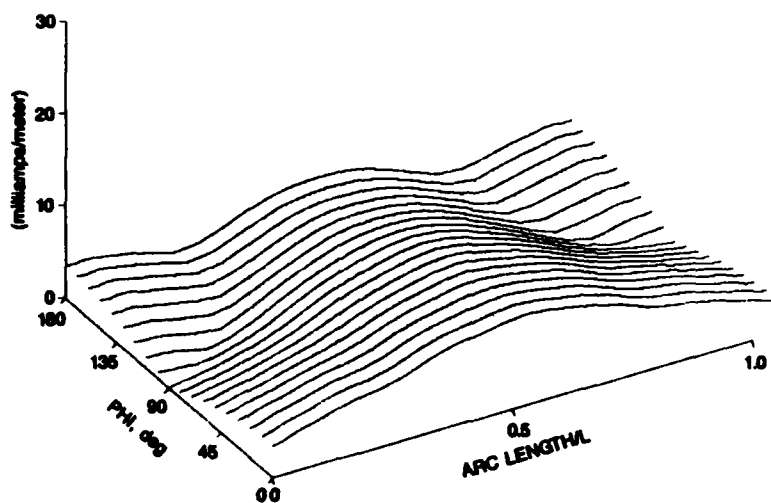
(a) Total currents
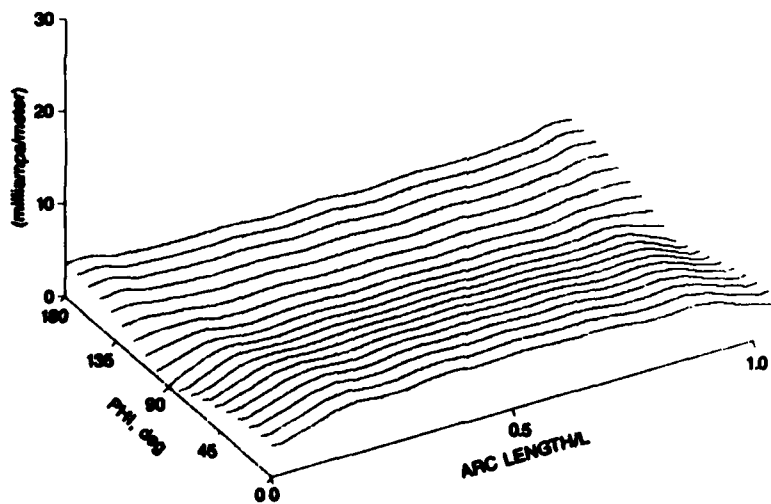
(b) Class 1 residual currents

Figure 4.8.   Surface currents on sphere-capped cylinder at a frequency
of C/L and an incident angle of θ = 90 degrees.

4-17
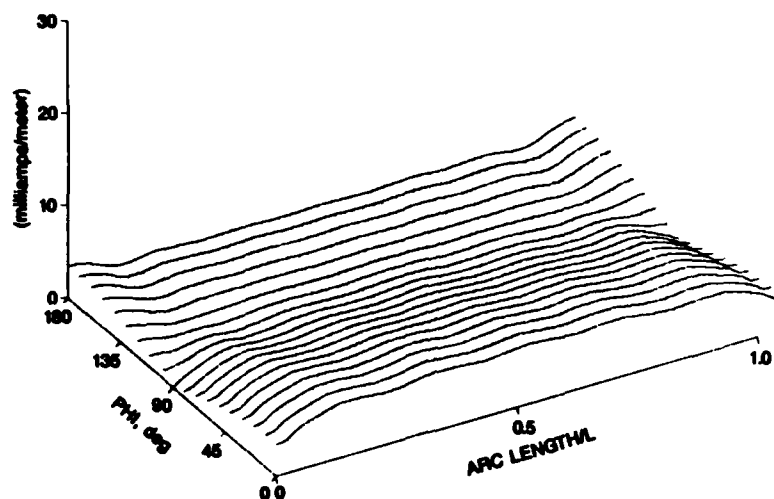
(c) Class 2 residual currents

Figure 4.8 (Cont.)
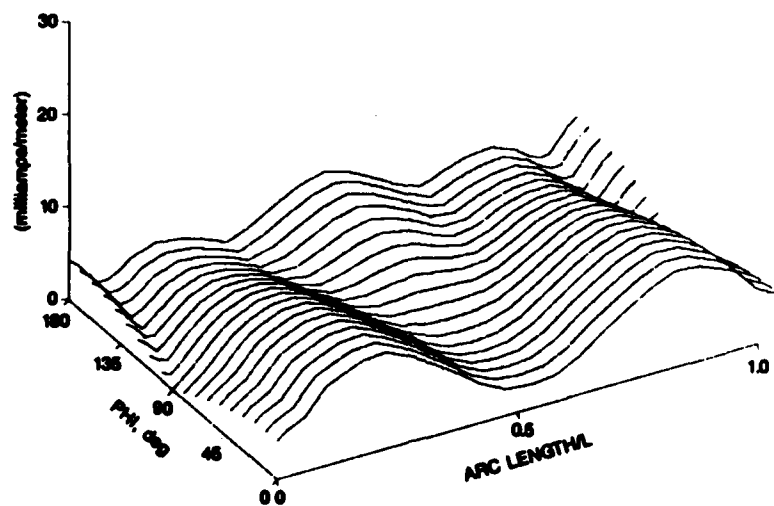
(a) Total currents

Figure 4.9. Surface currents on sphere-capped cylinder at a frequency of 3C/2L and an incident angle of θ = 90 degrees.

(b) Class 1 residual currents

(c) Class 2 residual currents

Figure 4.9 (Cont.)

Figure 4.10. φ-directed surface currents on sphere-capped cylinder at frequency of c/2L and an incident angle of θ = 0 degrees.

(a) t-directed currents
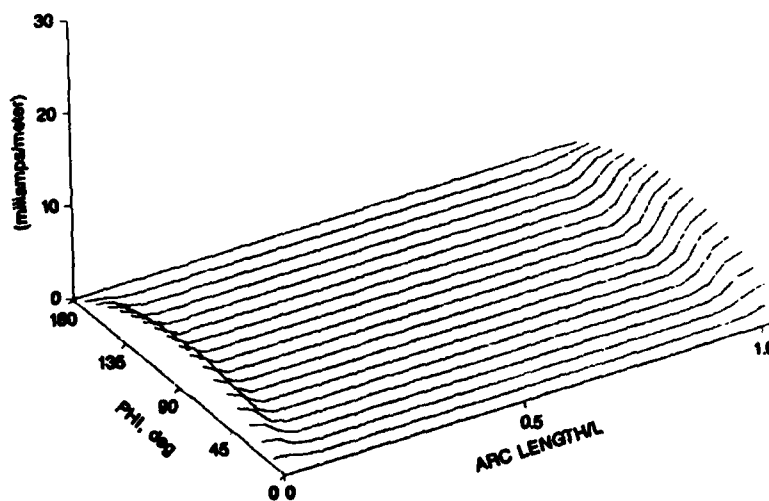
(b) φ-directed currents .

Figure 4.11.   Extended physical optics currents on sphere-capped
cylinder.

4-21

to an imbalance in the residual currents between the front and back sides of the cylinder.

One should probably not attempt to infer too much from the resemblance between residual and physical optics responses noted above since these responses become decidedly different as the cylinder radius approaches zero. For the filament scatterer, the physical optics response, which varies in direct proportion with the radius, is insignificant compared to the actual response given by Eqs. 2.8 through 2.10, which varies as $1/\log ka$. A refined local field solution similar to physical optics wherein the scatterer's curvature is brought to bear may provide a more accurate description of the residual currents.

Figure 4.12 shows the total, residual and physical optics monostatic radar cross sections (RCS) as a function of frequency for the cylinder with $L/D = 10$. The RCS is defined by

$$\sigma = \lim_{R \to \infty} 4\pi R^2 \left|\overline{E}^s\right|^2 \bigg/ \left|\overline{E}^i\right|^2$$

where $\overline{E}^s$ is the scattered electric field at the observation point, $\overline{E}^i$ is the incident electric field at the scatterer, and R is the distance to the far field. In Fig. 4.12, the RCS is expressed in decibels relative to L^2. The incident plane wave is assumed to be linearly polarized and θ-polarized. Figures 4.13 through 4.15 compare the θ components of various time-domain electric far field species. In each of these figures, the electric field is given in units of $(\sqrt{4\pi}\, R)^{-1} E_o L$ where E_o is the incident electric field magnitude. The time-domain incident field is given by
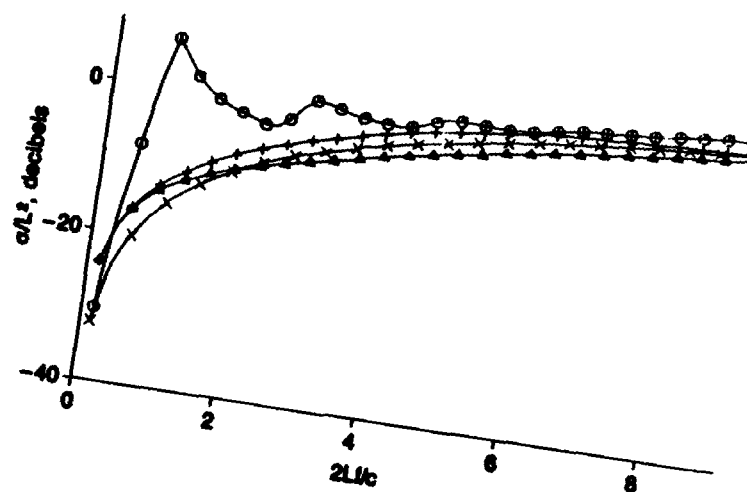
(a) L/D = 10 for θ = 90 degrees
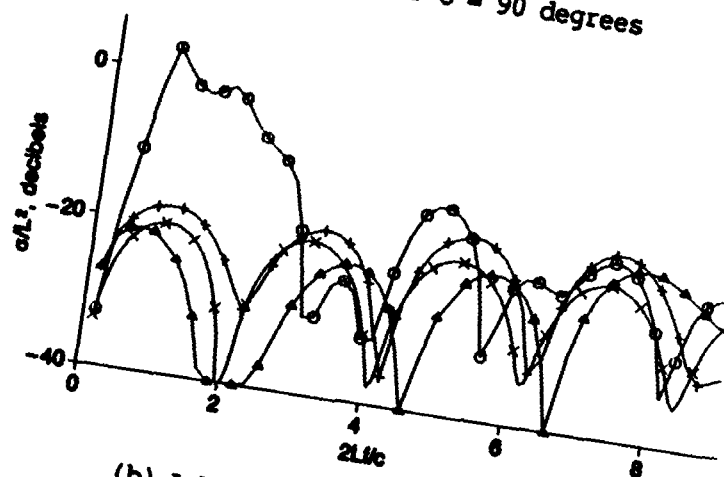
(b) L/D = 10 for θ = 60 degrees

Figure 4.12. Total (O), class 1 residual (Δ), class 2 residual (+), and true physical optics (X) RCS for sphere-capped cylinder.
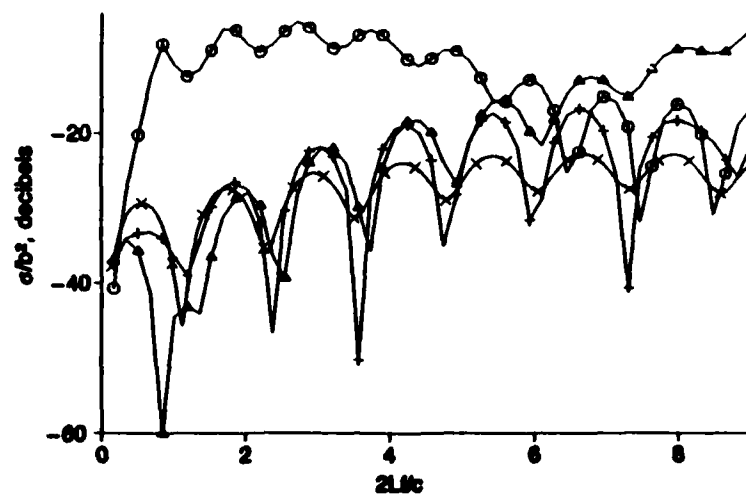
(c) L/D = 10 for θ = 30 degrees

Figure 4.12 (Cont.)
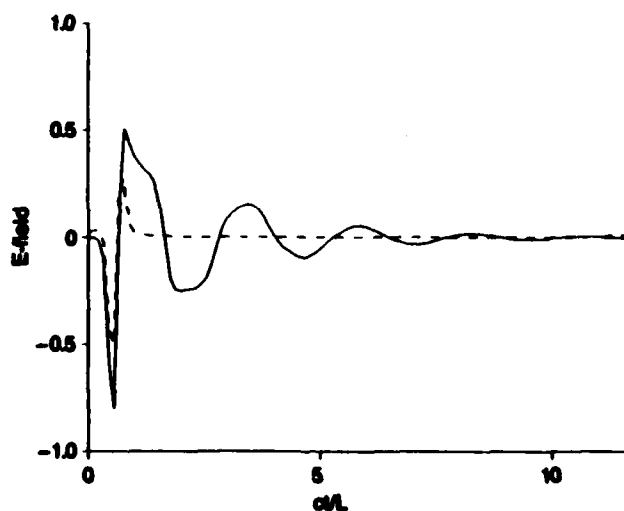
(a) θ = 90 degrees of sphere-capped cylinder with L/D = 10

Figure 4.13. Comparison of total (solid line) and class 2 residual (dashed line) electric far-field time histories.
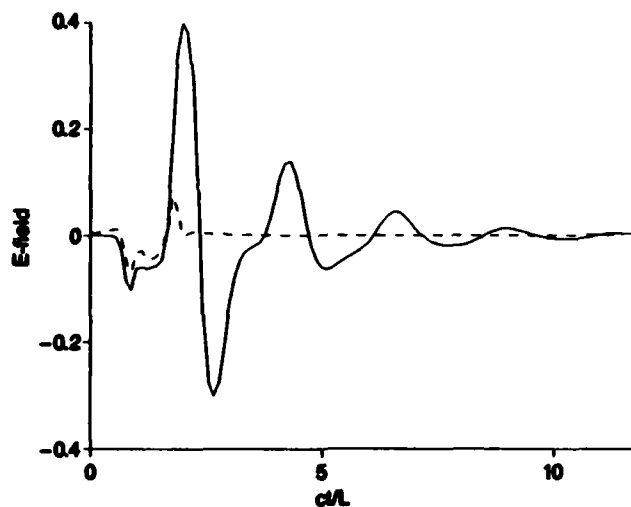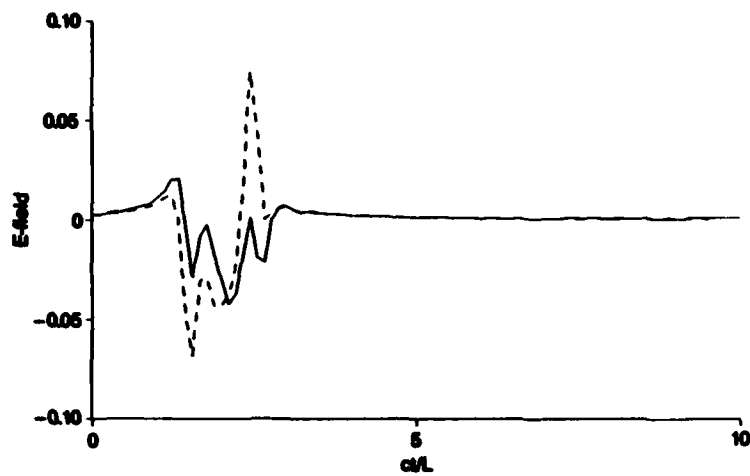
(b) Θ = 60 degrees of sphere–capped cylinder with L/D = 10
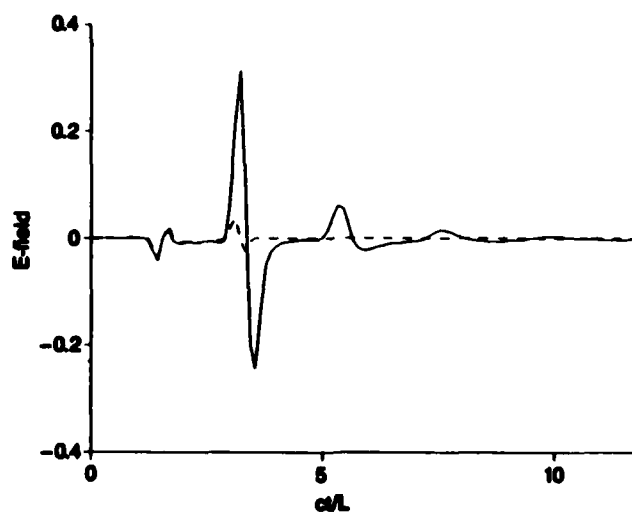
(c) Θ = 30 degrees of sphere–capped cylinder with L/D = 10

Figure 4.13 (Cont.)

4–25
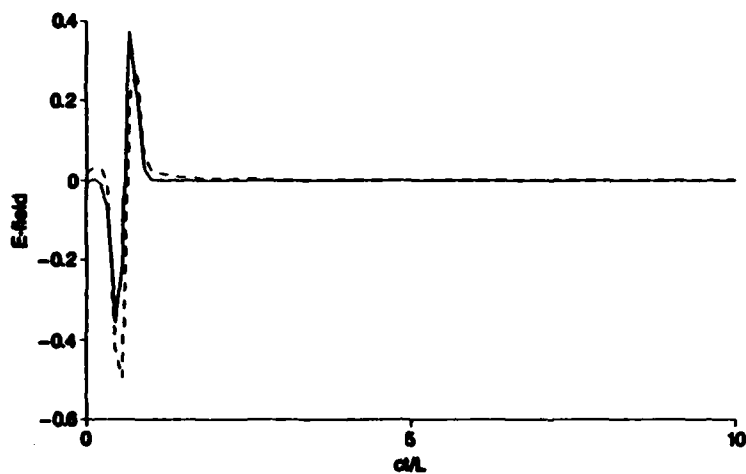
(a) Θ = 90 degrees of sphere-capped cylinder with L/D = 10
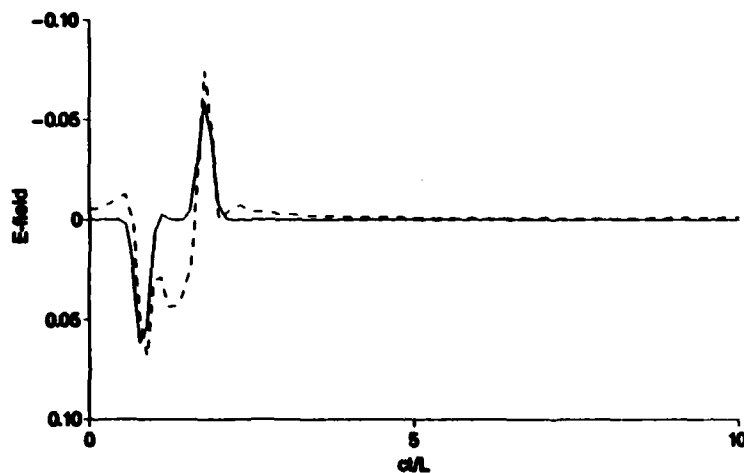
(b) Θ = 60 degrees of sphere-capped cylinder with L/D = 10

Figure 4.14. Comparison of true physical optics (solid line) with class 2 residual (dashed line) electric far-field time histories.
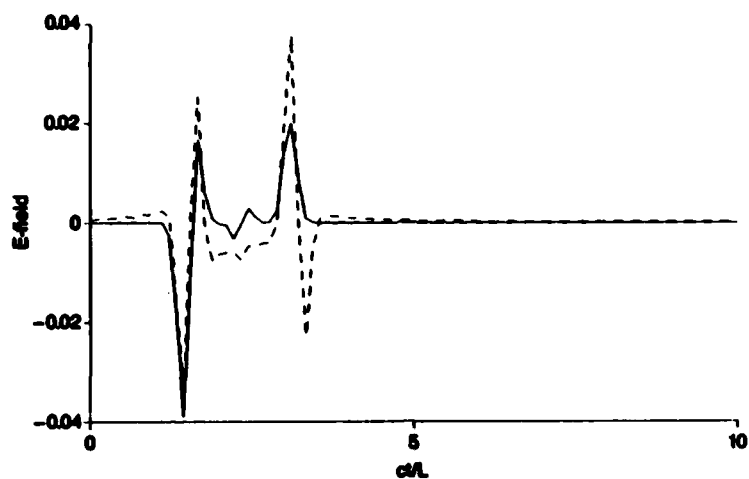
(c) Θ = 30 degrees of sphere-capped cylinder with L/D = 10

Figure 4.14 (Cont.)

(a) Θ = 90 degrees of sphere-capped cylinder with L/D = 10

Figure 4.15. Comparison of class 1 residual (solid line) with class 2
residual (dashed line) electric far-field time histories.

(b) θ = 60 degrees of sphere-capped cylinder with L/D = 10

(c) θ = 30 degrees of sphere-capped cylinder with L/D = 10

Figure 4.15 (Cont.)

$$\bar{E}^i(\bar{r},t) = \frac{2LE_o}{ct_o\pi^{3/2}} \ (\hat{x} \cos \theta - \hat{z} \sin \theta)$$

$$\times \exp[-(t - t_1 - \bar{p}\cdot\bar{r}/c)^2/t_o^2] \tag{4.4}$$

where $t_o = 0.1415L/c$, t_1 is an arbitrarily delay selected for conven-
ience in plotting, $\bar{p} = \bar{k}/k$, $k = |\bar{k}|$, $\bar{k}$ is the propagation vector of
the incident plane wave, and E_o is the incident electric field
strength. Note that the incident field has a Gaussian-pulse time his-
tory. Figures 4.16 through 4.19 show the corresponding results for the
cylinder with $L/D = 30$.

From the above results, the following observations can be made.
When the cylinder is relatively fat, the residual RCS shows a strong
resemblance to the physical optics RCS. As the cylinder becomes thin-
ner, the physical optics RCS becomes weaker relative to the residual
RCS. This last observation is consistent with the above-mentioned fact
that the physical optics response becomes insignificant in comparison to
the actual response as the cylinder radius approaches zero. Finally,
the class 2 residual time-domain responses closely resemble the aper-
iodic components in the filament responses of Sec. 2.

Figures 4.20 through 4.27 show the corresponding results for the
two loop scatterers. For the first loop, $b/a = 10$ and, for the
second, $b/a = 100$. These results provide another example of early-
time components in transient scattering responses and tend to corrobor-
ate the above observations for the cylinder's responses. The excitation
for all the loop responses is a ϕ-polarized plane wave incident from
various directions. The incident electric field is always parallel to
the plane of the loop. Figures 4.21 through 4.23 and 4.25 through 4.27
show the ϕ components of various time-domain electric far field spe-
cies. In each of these figures, the electric field is in units of
$(\sqrt{4\pi}R)^{-1}E_ob$. The time-domain incident field is given by
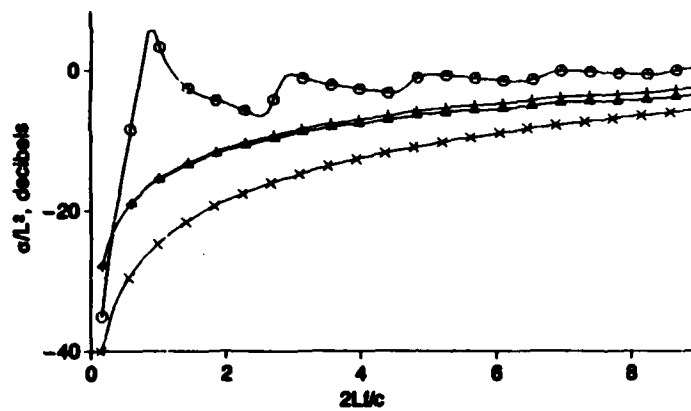
(a) L/D = 30 for θ = 90 degrees
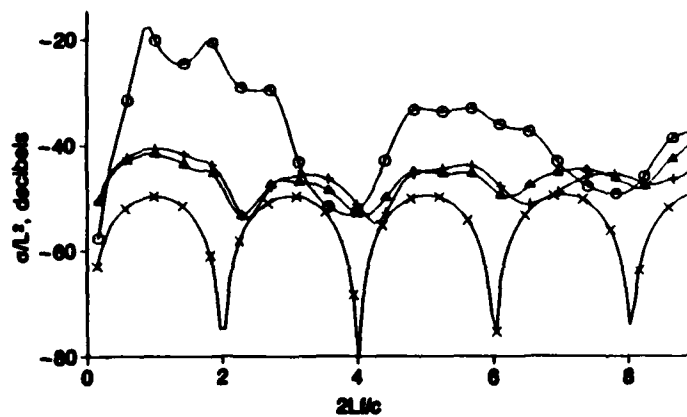
(b) L/D = 30 for θ = 60 degrees

Figure 4.16. Total (O), class 1 residual (Δ), class 2 residual (+), and true physical optics (X) RCS for sphere-capped cylinder.
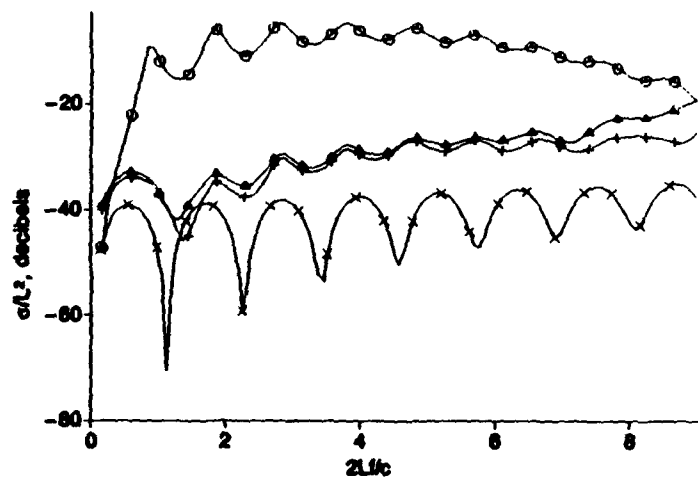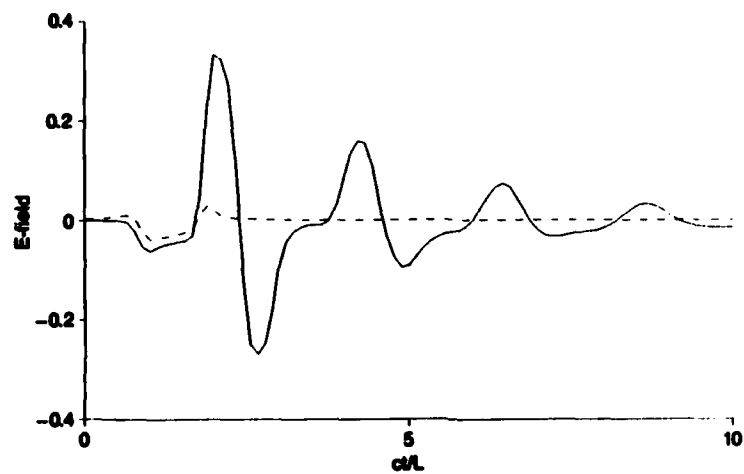
(c) L/D = 30 for θ =30 degrees

Figure 4.16 (Cont.)
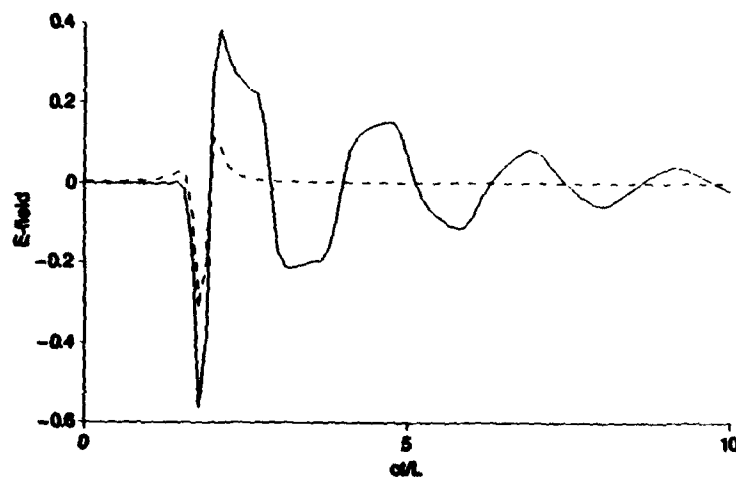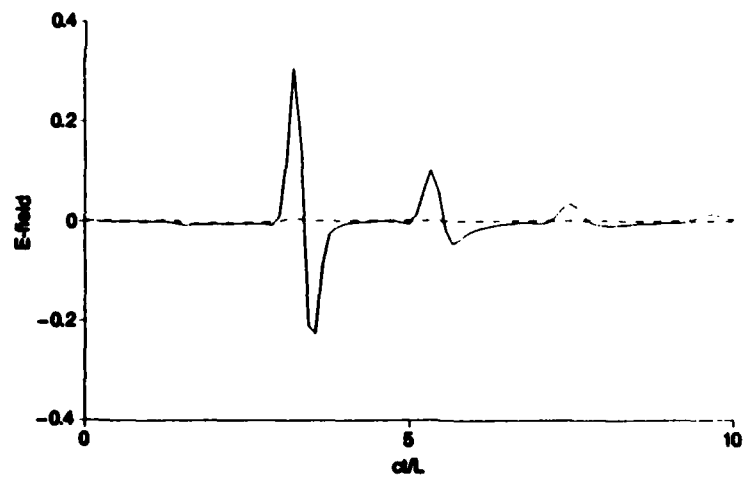

(a) θ = 90 degrees of sphere-capped cylinder with L/D = 30

Figure 4.17. Comparison of total (solid line) and class 2 residual
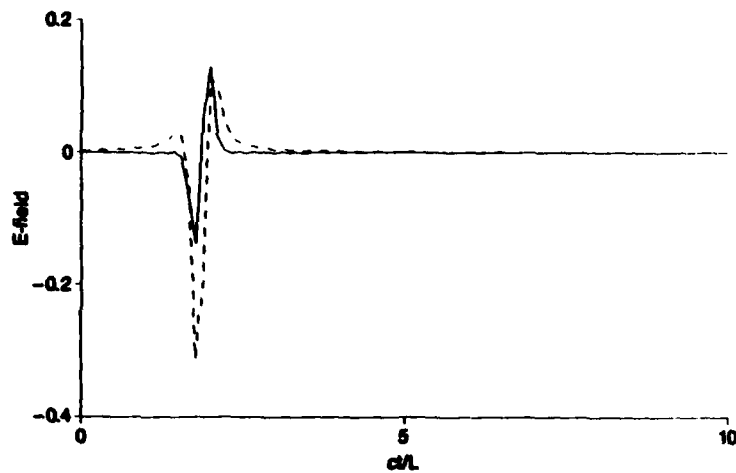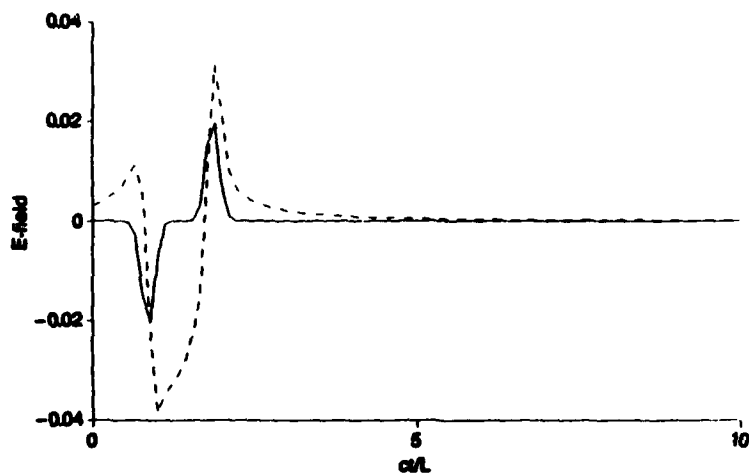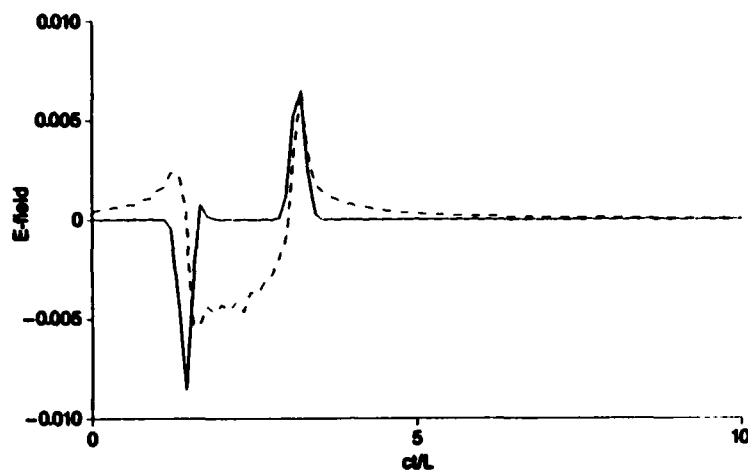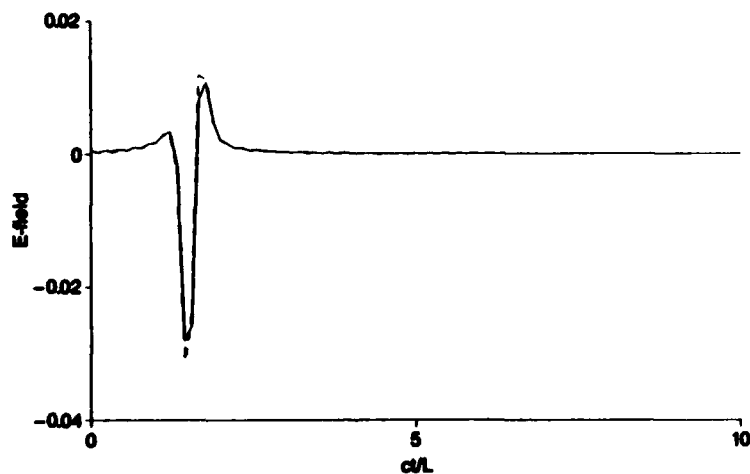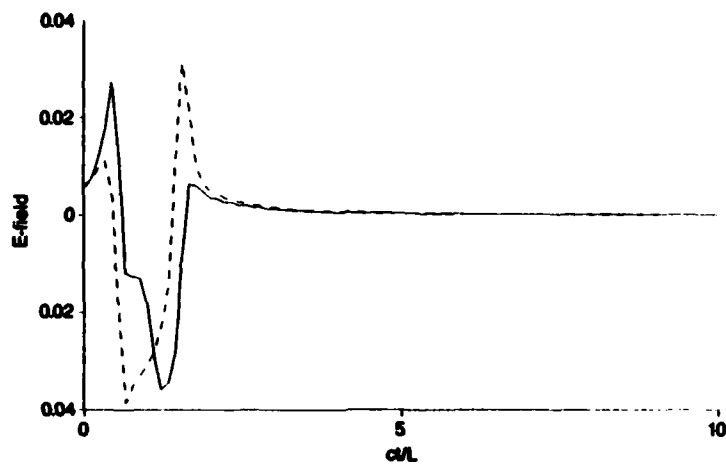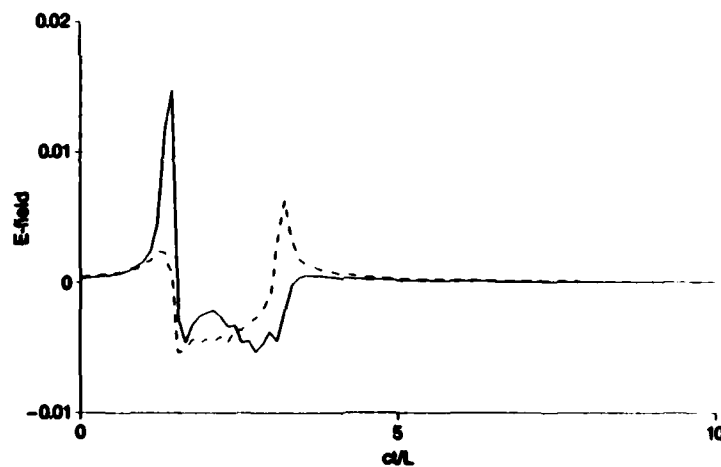(dashed line) electric far-field time histories.

(b) θ = 60 degrees of sphere-capped cylinder with L/D = 30

(c) θ = 30 degrees of sphere-capped cylinder with L/D = 30

Figure 4.17 (Cont.)

(a) θ = 90 degrees of sphere-capped cylinder with L/D = 30
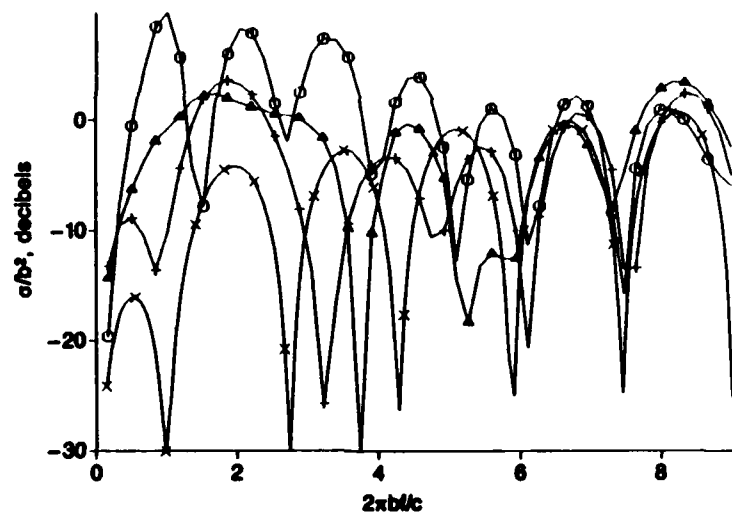

(b) θ = 60 degrees of sphere-capped cylinder with L/D = 30

Figure 4.18.   Comparison of true physical optics (solid line) and class
2 residual (dashed line) electric far-field time
histories.

(c) θ = 30 degrees of sphere-capped cylinder with L/D = 30

Figure 4.18 (Cont.)

(a) θ = 90 degrees of sphere-capped cylinder with L/D = 30

Figure 4.19.   Comparison of class 1 residual (solid line) with class 2 residual (dashed line) electric far-field time histories.

(b) θ = 60 degrees of sphere-capped cylinder with L/D = 30

(c) θ = 30 degrees of sphere-capped cylinder with L/D = 30

Figure 4.19 (Cont.)

4-35
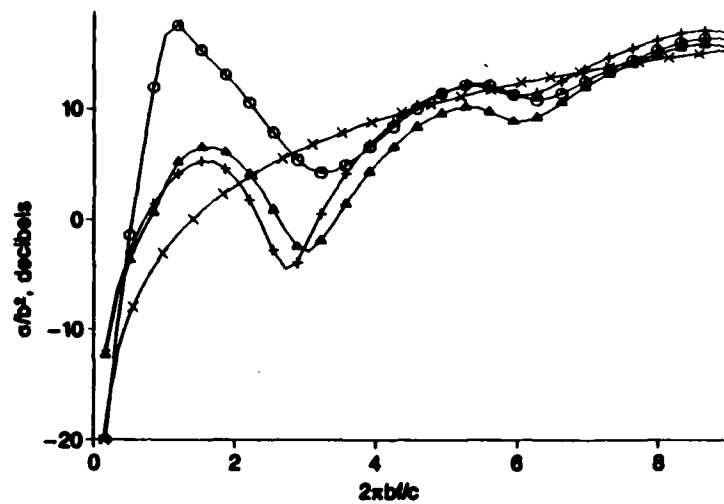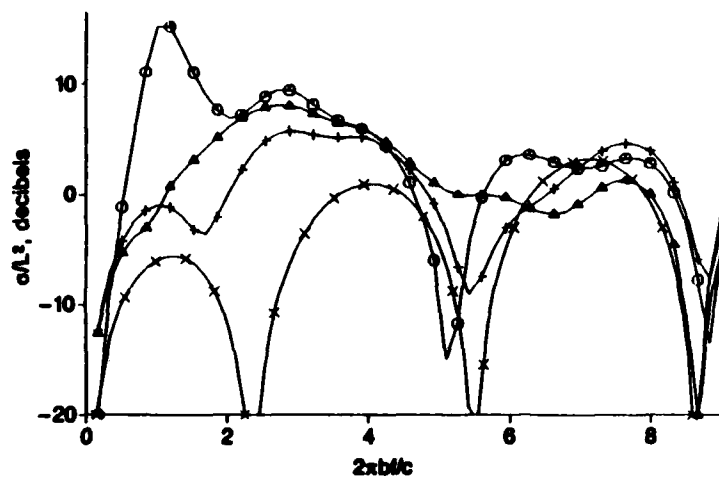
(a) θ = 0 degrees

(b) θ = 30 degrees

Figure 4.20.   Total (O), class 1 residual (Δ), class 2 residual (+), and true physical optics (X) RCS for loop with b/a = 10.

4-36
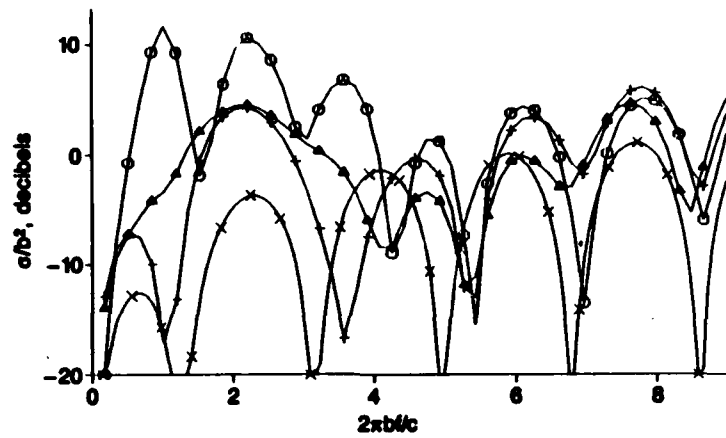
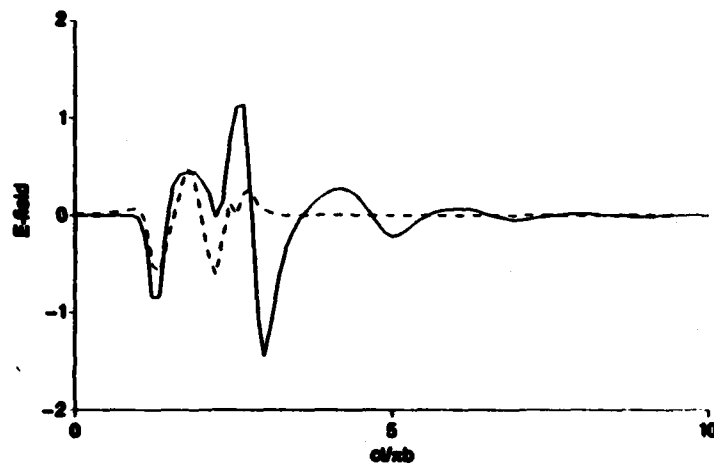(c) θ = 60 degrees

(d) θ = 90 degrees

Figure 4.20 (Cont.)

4-37
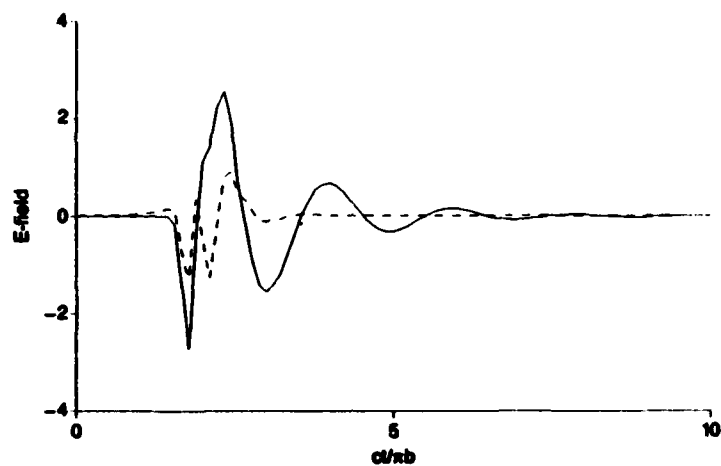
(a) θ = 0 degrees of loop with b/a = 10
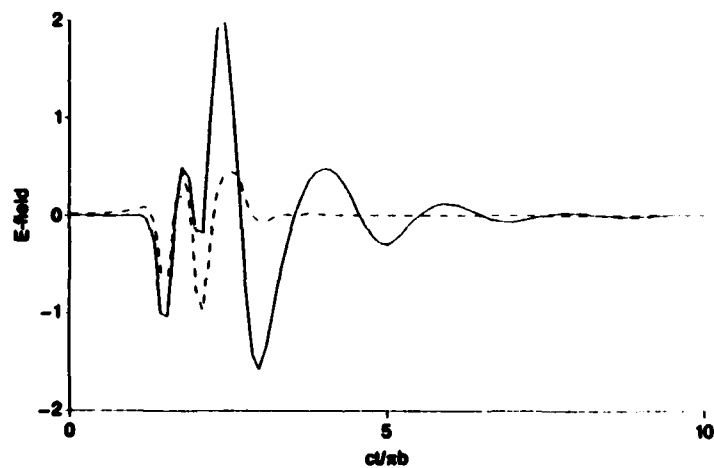
(b) θ = 30 degrees of loop with b/a = 10

Figure 4.21. Comparison of total (solid line) and class 2 residual
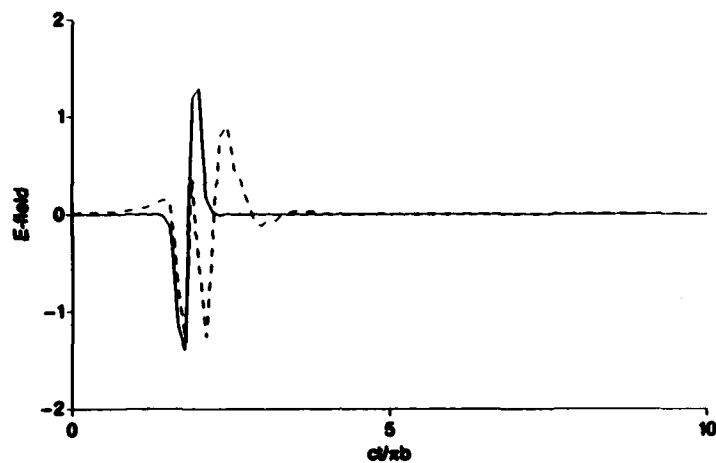(dashed line) electric far-field time histories.
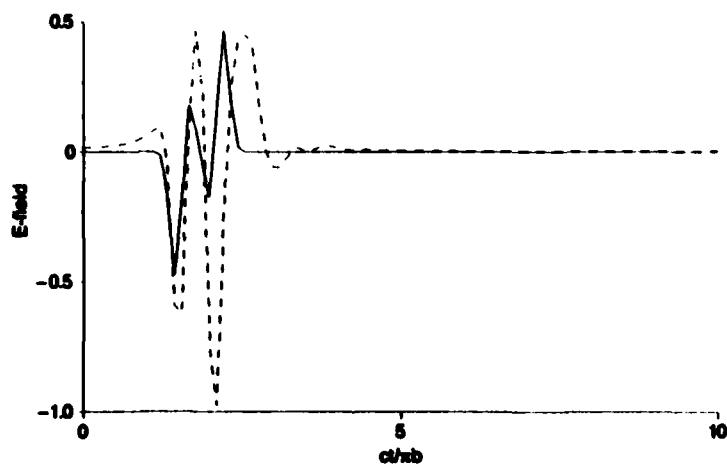
(c) θ = 60 degrees of loop with b/a = 10

(d) θ = 90 degrees of loop with b/a = 10

Figure 4.21 (Cont.)

4-39

(a) θ = 0 degrees of loop with b/a = 10

(b) θ = 30 degrees of loop with b/a = 10

Figure 4.22.   Comparison of true physical optics (solid line) and class
2 residual (dashed line) electric far-field time
histories.

(c) $\theta = 60$ degrees of loop with b/a = 10

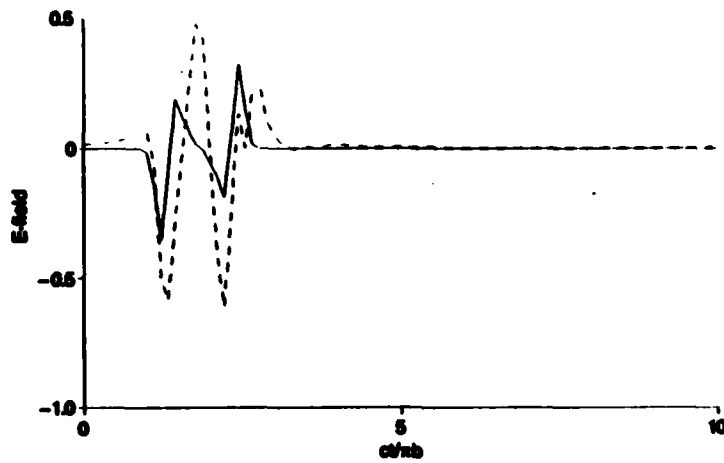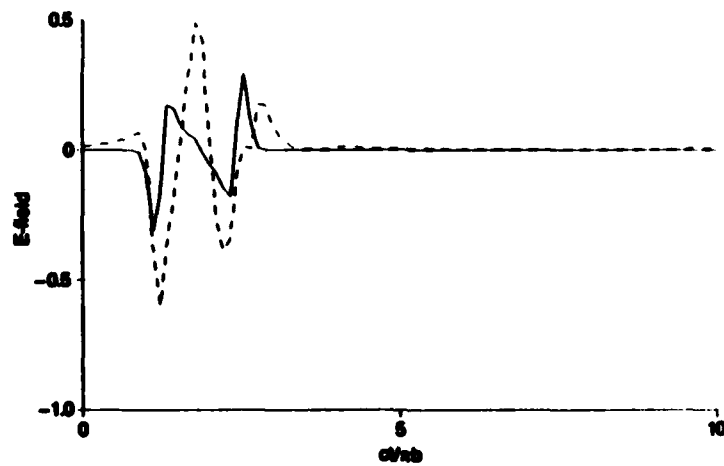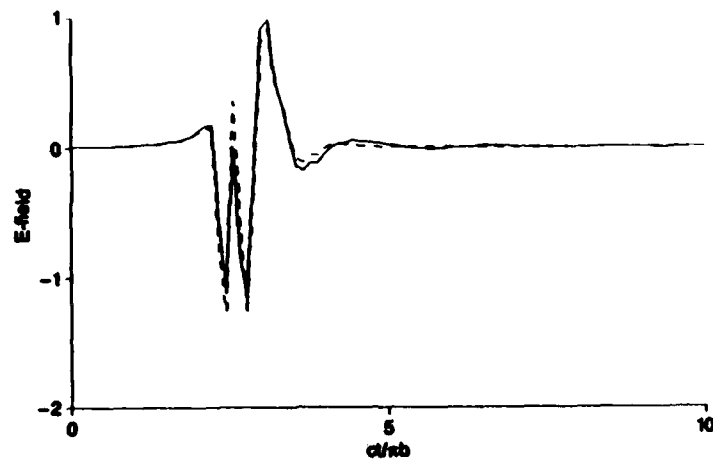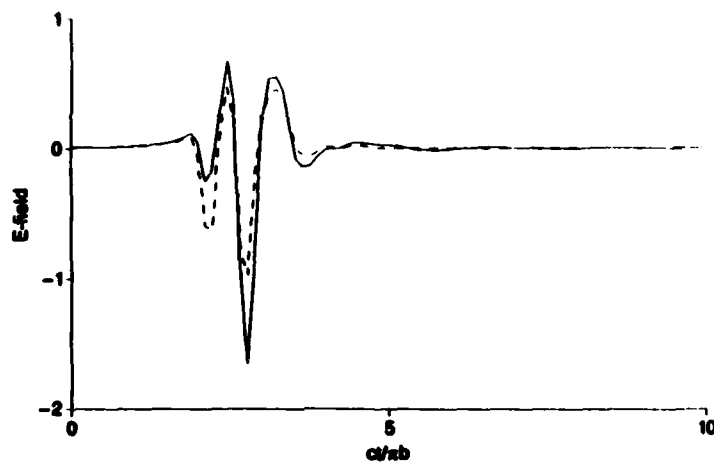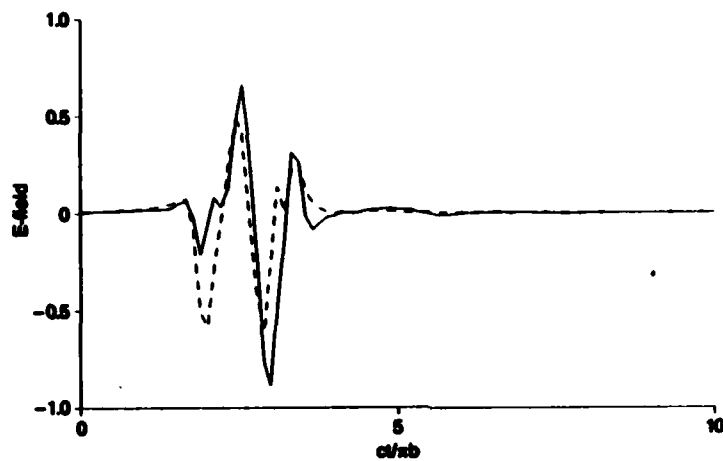(d) $\theta = 90$ degrees of loop with b/a = 10

Figure 4.22 (Cont.)

(a) θ = 0 degrees of loop with b/a = 10

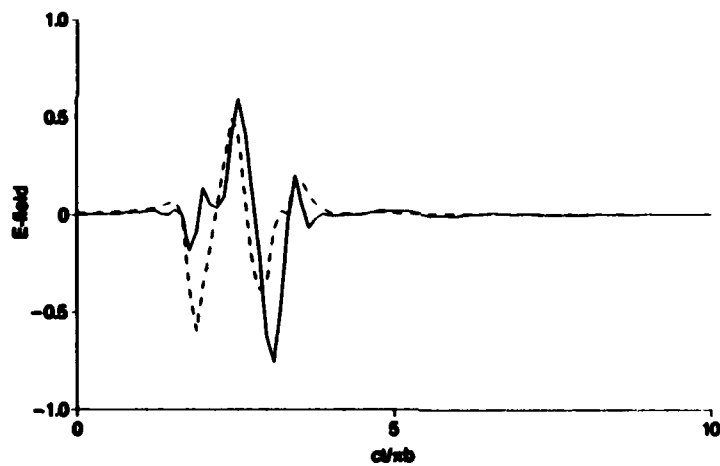(b) θ = 30 degrees of loop with b/a = 10

Figure 4.23. Comparison of class 1 residual (solid line) with class 2
residual (dashed line) electric far-field time histories.

(c) θ = 60 degrees of loop with b/a = 10

(d) θ = 90 degrees of loop with b/a = 10

Figure 4.23 (Cont.)

(a) b/a = 100 for θ = 0 degrees

(b) b/a = 100 for θ = 30 degrees

Figure 4.24.   Total (O), class 1 residual (Δ), class 2 residual (+), and
true physical optics (X) RCS for loop.

4-44

(c) b/a = 100 for θ = 60 degrees
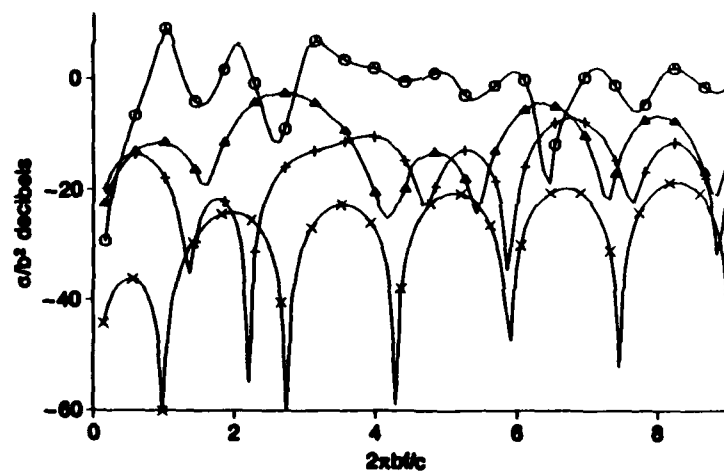
(d) b/a = 100 for θ = 90 degrees

Figure 4.24 (Cont.)

4-45
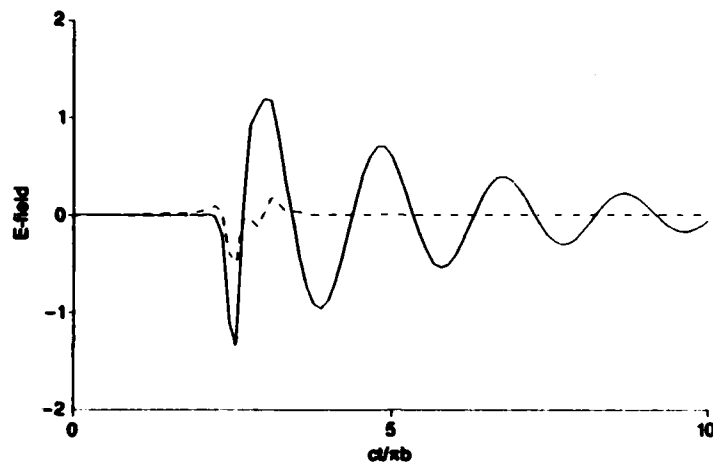
(a) θ = 0 degrees of loop with b/a = 100
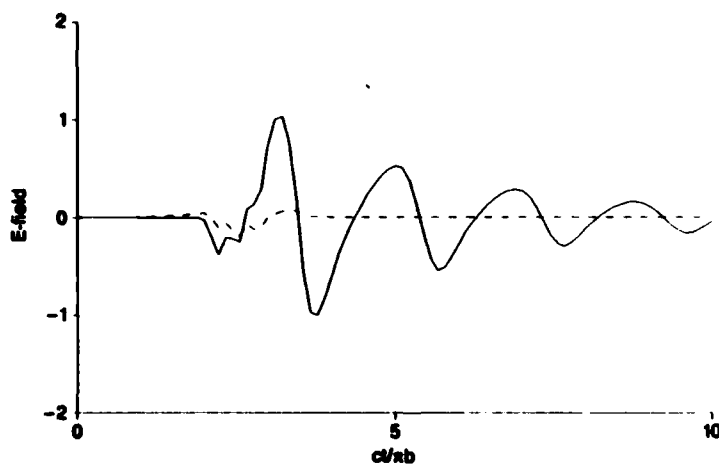
(a) θ = 30 degrees of loop with b/a = 100

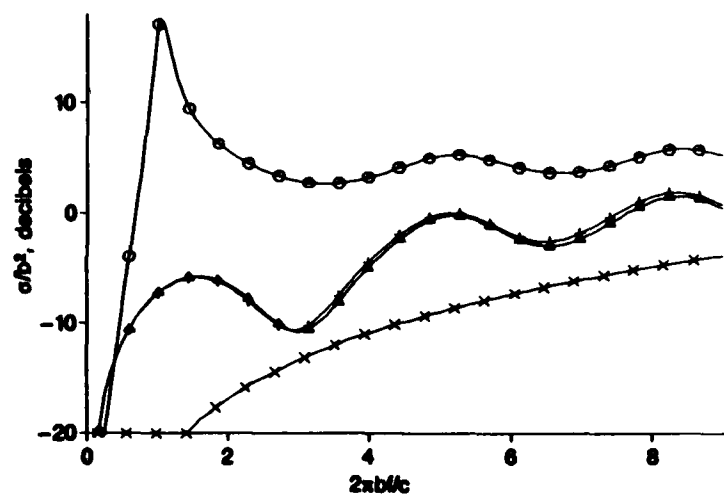Figure 4.25. Comparison of total (solid line) and class 2 residual (dashed line) electric far-field time histories.

4-46
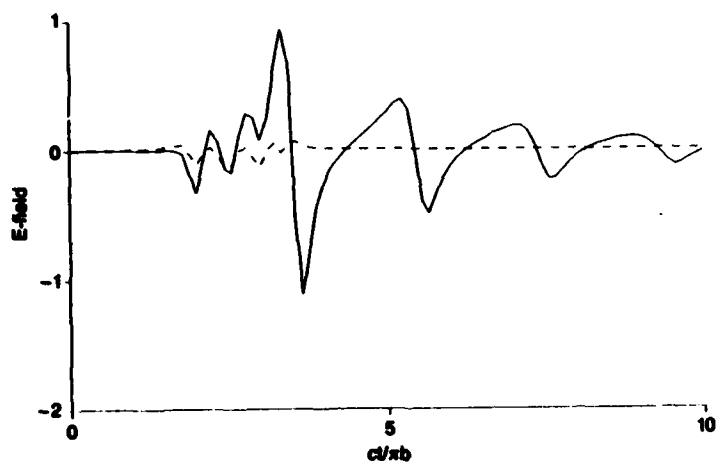
(c) θ = 60 degrees of loop with b/a = 100

(d) θ = 90 degrees of loop with b/a = 100

Figure 4.25 (Cont.)
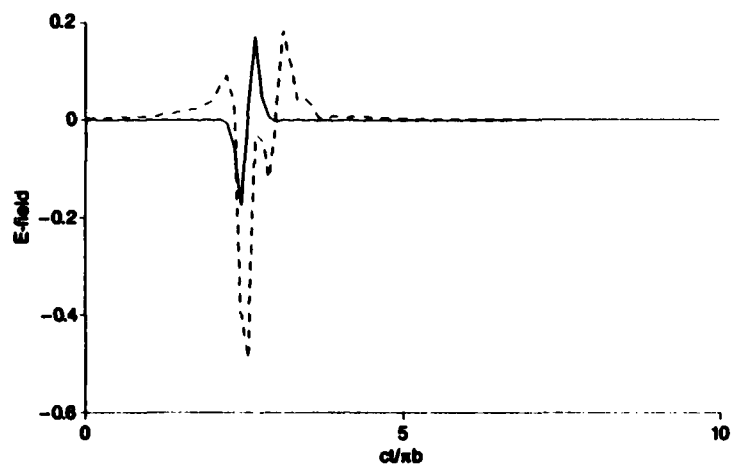
(a) θ = 0 degrees of loop with b/a = 100
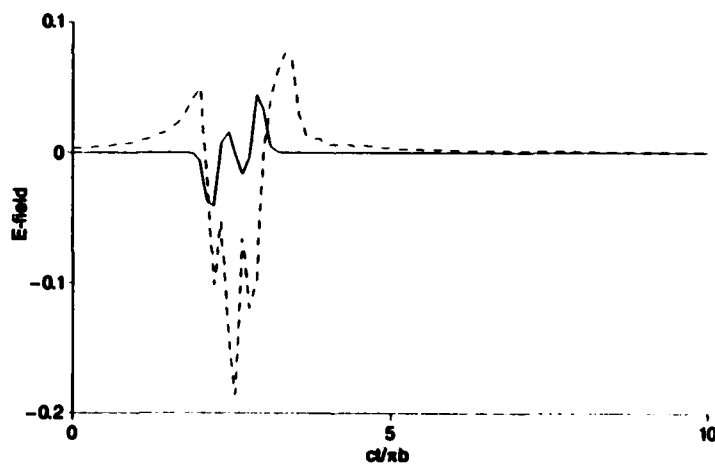
(b) θ = 30 degrees of loop with b/a = 100

Figure 4.26. Comparison of true physical optics (solid line) and class 2 residual (dashed line) electric far-field time histories.

4-48
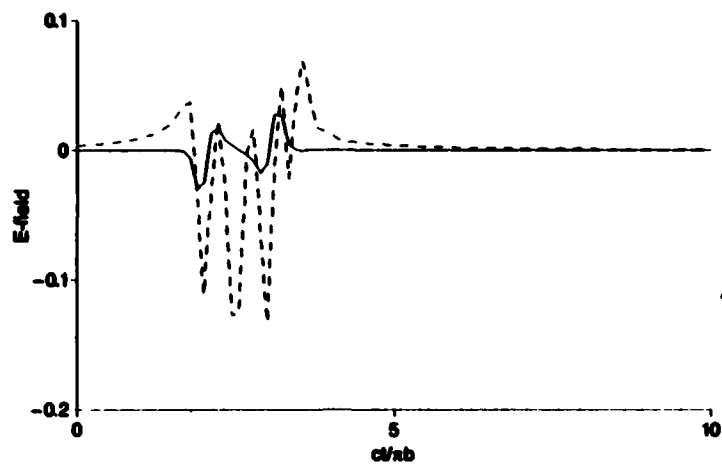
(c) θ = 60 degrees of loop with b/a = 100

(d) θ = 90 degrees of loop with b/a = 100

Figure 4.26 (Cont.)

4-49
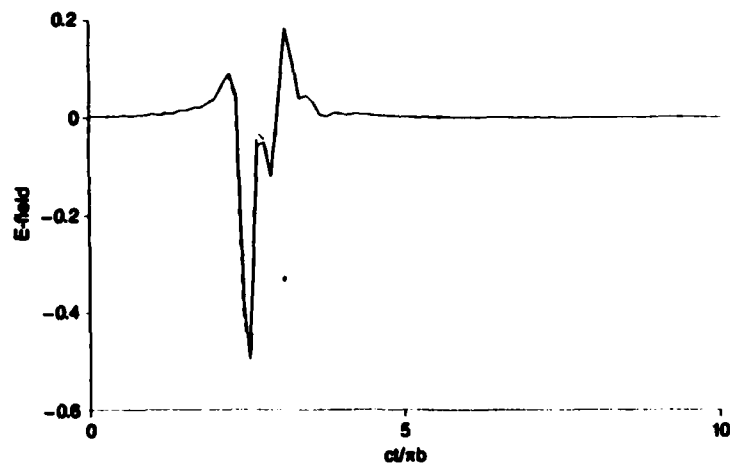
(a) θ = 0ʼ degrees of loop with b/a = 100
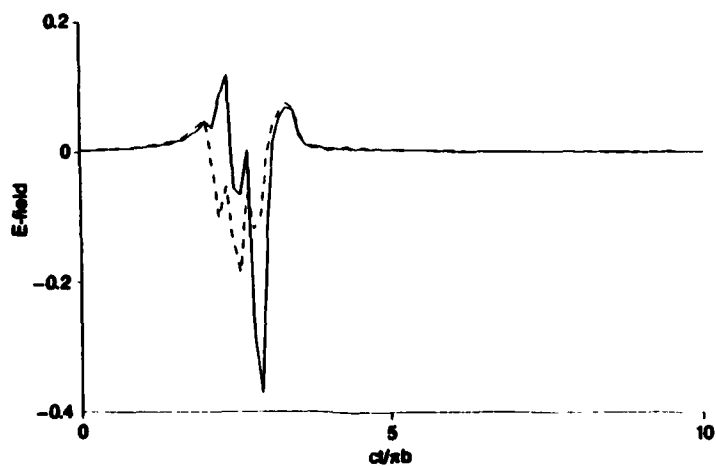
(b) θ = 30 degrees of loop with b/a = 100

Figure 4.27.   Comparison of class 1 residual (solid line) and class 2
residual (dashed line) electric far-field time
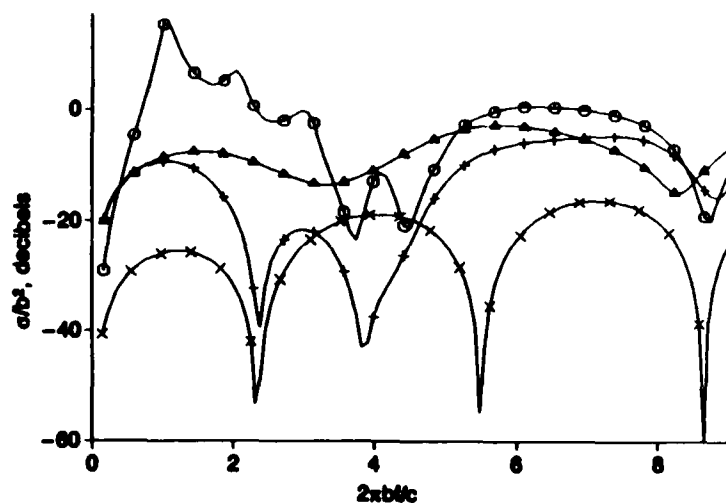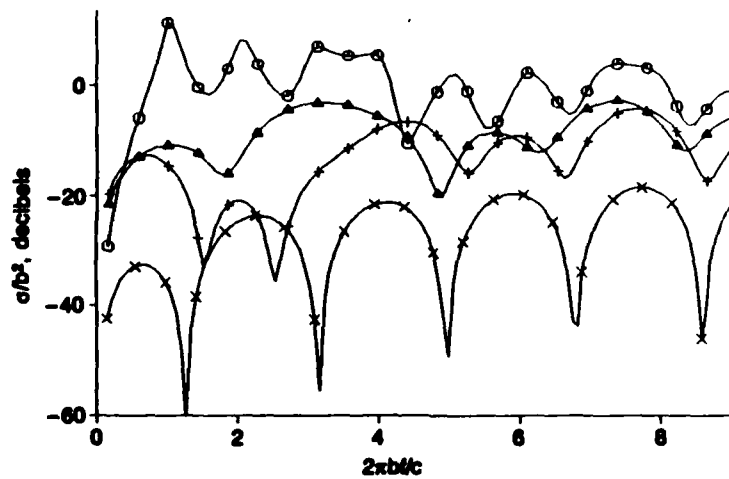histories.

(c) Θ = 60 degrees of loop with b/a = 100

(d) Θ = 90 degrees of loop with b/a = 100

Figure 4.27 (Cont.)

$$\mathbf{E}^i(\bar{r},t) = \frac{2b\mathbf{E}_o}{ct_o\pi^{1/2}}\,\hat{\phi} \times \exp[-(t - t_1 - \bar{p}\cdot\bar{r}/c)^2/t_o^2] \qquad (4.5)$$

where $t_o = 0.4444b/c$ and the other quantities in Eq. 4.5 are defined as in Eq. 4.4.

5   CONCLUSIONS

The results of this effort indicate that, in a practical SEM re-
presentation for general scatterers, a quasi-entire function is required
in addition to a pole series constructed from the dominant resonances of
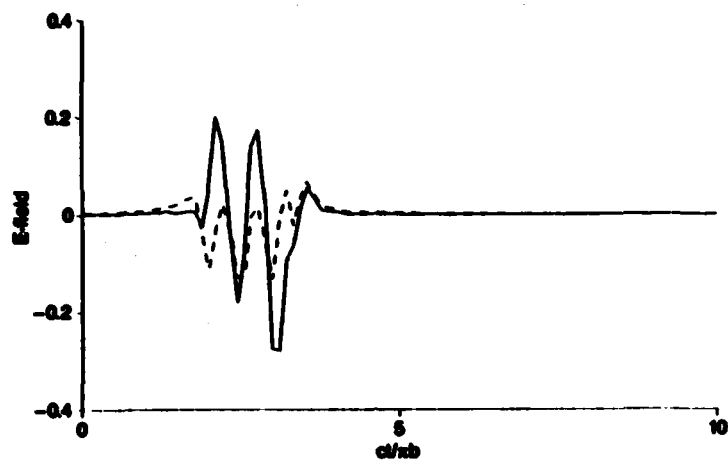the scatterer. The quasi-entire function may be regarded as a forced
component in the same spirit as the familiar forced components in the
responses of circuits. The forced components may find a concise
description in a form similar to the extended physical optics response
with, perhaps, refinements to account for the scatterer's curvature.
One refined physical optics solution has already been used.[16,17] The
description might also assume a ray-theoretic form.[2,3]

The authors cannot, unfortunately, apply the completeness argument
of Sec. 3 with absolute rigor to transient responses of general scat-
terers since we know very little about the distribution of poles in the
s-plane for general scatterers. A possible rigorous argument might be
found by proceeding from the completeness of the eigen modes and their
close, but complicated relation to the natural modes.[18]

It is interesting to notice that the forced components are con-
structed from poles, i.e., aspect angle independent features. However,
resolving individual pole terms within the forced components is well-
nigh impossible. Given the nature of this component, it seems doubtful
that any other aspect independent features can be found. Target identi-
fication using information within the forced response, therefore, would
almost certainly require knowledge of the target's orientation which can
frequently be obtained from radar tracking information.

Realization of resonance-based target identification hinges on the
existence of dominant resonances and proper processing to deal with the
forced response. Ideally, information within the forced response would
also be exploited for identification. This effort has clarified the
nature of forced responses in transient scattering and has shown their

5-1

close relation to the SEM entire function. Armed with this information, it should now be possible to explore procedures for exploiting both dominant resonances and the forced response for target identification and other applications.

REFERENCES

1. C.E. Baum, "On the Singularity Expansion Method for the Solution of Electromagnetic Interaction Problems," AFWL Interaction Note 88, Air Force Weapons Laboratory, December 11, 1971.

2. E. Heyman and Leopold B. Felsen, "Wavefront Interpretation of the Singularity Expansion Method," IEEE Transactions on Antennas and Propagation, Vol. AP-33, No. 7, July 1985, pp. 706-718.

3. H. Überall and G.C. Gaunaurd, "Relation Between the Ringing of Resonances and Surface Waves in Radar Scattering," IEEE Transactions on Antennas and Propagation, Vol. AP-32, No. 10, October 1984, pp. 1071-1079.

4. M.A. Morgan, "Singularity Expansion Representations of Fields and Currents in Transient Scattering," IEEE Transactions on Antennas and Propagation, Vol. 32, No. 5, May 1984, pp. 466-473.

5. L.W. Pearson, "A Note on the Representation of Scattered Fields as a Singularity Expansion," IEEE Transactions on Antennas and Propagation, Vol. AP-32, No. 5, May 1984, pp. 520-521.

6. M.A. Morgan, "Response to Comments Regarding SEM Representations," IEEE Transactions on Antennas and Propagation, Vol. AP-33, No. 1, January 1985, p. 120.

7. W.R. Smythe, Static and Dynamic Electricity, Third Edition, McGraw-Hill, New York, 1968.

8. J.A. Stratton, Electromagnetic Theory, McGraw-Hill, New York, 1941.

9. R.F. Harrington, Time-Harmonic Electromagnetic Fields, McGraw-Hill, New York, 1961.

10. Y.M. Chen and J.B. Keller, "Current on and Input Impedance of a Cylindrical Antenna," Journal of Research, National Bureau of Standards, Vol. 66D, No. 1, January-February 1962, pp. 15-21.

11. J.R. Auton, "BRFD--An SEM Scattering Code for General Bodies of Revolution," General Research Corporation, Santa Barbara, CA (in preparation).

12. M.L. VanBlaricum and R. Mittra, "A Technique for Extracting the Poles and Residues of a System Directly From its Transient Response," IEEE Transactions on Antennas and Propagation, Vol. AP-23, November 1975, pp. 777-781.

13. R.F. Harrington, Field Computation by Moment Methods, McMillan, New York, 1968.

14. C.E. Baum, "Emerging Technology for Transient and Broad-Band Analysis and Synthesis of Antennas and Scatterers," Proceedings of the IEEE, Vol. 64, No. 11, November 1974, pp. 1596-1616.

15. C.E. Baum, "The Singularity Expansion Method," Chapter 3 of Transient Electromagnetic Fields, L.B. Felsen (Ed.), Springer-Verlag, New York, 1976.

16. B. Foo, S.K. Chaudhuri, and W. Boerner, "A High Frequency Inverse Scattering Model to Recover the Specular Point Curvature From Polarimetric Scattering Matrix Data," IEEE Transactions on Antennas and Propagation, Vol. AP-32, No. 11, November 1984, pp. 1174-1178.

17. C.L. Bennett, A.M. Auckenthaler, R.S. Smith, and J.D. DeLorenzo, "Space-Time Integral Equation Approach to Large Body Scattering Problems," Sperry Research Center, Sudbury, MA, Final Report on Contract F30602-71-C-0162, AD 763794, May 1973.

18. C.E. Baum, "On the Eigenmode Expansion Method for Electromagnetic Scattering and Antenna Problems, Part I: Some Basic Relations for Eigenmode Expansions, and their Relation to the Singularity Expansion," AFWL Interaction Note 229, Air Force Weapons Laboratory, January 13, 1975.

19. M.L. VanBlaricum, Techniques for Extracting the Complex Resonances of a System Directly from its Transient Response, Ph.D. Dissertation, December 1975, University of Illinois, Department of Electrical Engineering.

APPENDIX A

POLE SERIES REPRESENTATIONS OF AN EXPONENTIAL

Here it is shown that

$$\exp(z) \simeq P_N(z) \tag{A.1}$$

where

$$P_N(z) = \exp(\gamma) \prod_{i=1}^{N} N(z_i - z)^{-1} \tag{A.2}$$

and

$$\gamma = \frac{1}{N} \sum_{i=1}^{N} (z_i - N) \tag{A.3}$$

Taking the logarithm of Eq. A.2 gives

$$\log P_N = \gamma - \sum_{i=1}^{N} \log \frac{z_i - z}{N} = z + \sum_{i=1}^{N} O\left[\left(\frac{z_i - z}{N} - 1\right)^2\right] \tag{A.4}$$

If $|z| \ll N$ and $|z_i - N| \ll N$ for all i, then Eq. A.4 becomes

$$\log P_N \simeq z$$

which is equivalent to Eq. A.1. If, in addition,

$$1 \gg \frac{1}{N} \left| \sum_{i=1}^{N} (z_i - N) \right|$$

then

$$\exp(z) = \prod_{i=1}^{N} N(z_i - z)^{-1}$$

APPENDIX B

APPROXIMATION OF A PULSE FUNCTION

The pulse function $g(t) = u(t) - u(t-1)$, where $u(t)$ is the unit step function, is to be approximated by

$$f(t) = \sum_{i=1}^{N} A_i t^{i-1} \exp(-Nt)$$

on the interval (o, ∞). The approximation criterion is the integrated square error:

$$E = \int_o^\infty \left[g - \sum_i A_i t^{i-1} \exp(-Nt) \right]^2 dt$$

Setting the partial derivatives of E with respect to each A_i to zero provides the system of equations,

$$F_j = \sum_{i=1}^{N} A_i E_{ij} \qquad j = 1, \ldots, N \tag{B.1}$$

which can be solved for the A_i that minimize E. In Eq. B.1,

$$F_j = \int_o^1 t^{j-1} \exp(-Nt) \, dt,$$

$$E_{ij} = \int_0^\infty t^{i+j-2} \exp(-2Nt) \, dt$$

The F_j and E_{ij} are evaluated analytically.

APPENDIX C

METHODS FOR CONSTRAINING PRONY'S ALGORITHM

In the implementation of Prony's method, an nth order polynomial is solved for its roots. The order of the polynomial, N, is the number of poles being sought in the transient data. If the coefficients of the polynomial are denoted as α then the polynomial can be expressed as per Ref. 19, as

$$\alpha_0 + \alpha_1 z^1 + \alpha_2 z^2 + \ldots + \alpha_N z_N = 0 \qquad (C.1)$$

where α_N is usually set equal to unity. The N roots, z_i, are defined as

$$z_i = e^{\Delta t s_i} \qquad (C.2)$$

with s_i being the poles sought, and Δt being the time step size used in the analysis.

If the value of one or more of the poles is known—that is, we know some of the z_i —then the z_i can be substituted into Eq. C.1. For example, if s_i or z_i is known, then Eq. C.1 can be written as

$$\alpha_0 + \alpha_1 z_i + \alpha_2 z_i^2 + \ldots + \alpha_N z_i^N = 0 \qquad (C.3)$$

The $N + 1$ polynomial coefficients α are solved for in Prony's method by solution of the difference equation
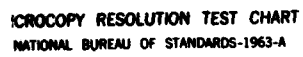
MICROCOPY RESOLUTION TEST CHART
NATIONAL BUREAU OF STANDARDS-1963-A

$$\sum_{p=0}^{N-1} \alpha_p I_{p+K} = -I_{N+K}, \quad k = 0, 1, \ldots, \gamma - 1, \quad \gamma = M - N \qquad (C.4)$$

The I_{p+K} and I_{N+K} are the samples of the transient signal being ana-lyzed and M is the total number of samples being used. The value of M must be at least equal to $2N$ to give N sets of equations in the N unknowns α_p. However, if the value of a pole is known, then one of the N equations can be Eq. C.3 and $N-1$ equations of the form of Eq. C.4 can be written.

If L poles are known a priori, the L equations of the form of Eq. C.3 can be written as

$$\sum_{p=0}^{N-1} \alpha_p z_\ell^p = -z_\ell^N \qquad , \quad \ell = 1, 2, \ldots, L \qquad (C.5)$$

and $\gamma = M - N - L$ equations can be written in the form of Eq. C.4 as

$$\sum_{p=0}^{N-1} \alpha_p I_{p+K} = -I_{K+N} \quad , \quad k = 0, 1, \ldots, \gamma - 1 \quad , \quad \gamma = M - N - L \qquad (C.6)$$

Hence, there are still $\gamma = M - N$ total equations to solve for the N values of α_p, however, the system is constrained by the knowledge of the location of L poles. As is usually done in Prony's method, if $M = 2N$, then the set of equations is inverted and solved. If $M > 2N$, then a pseudo-inverse procedure is used.

Using the matrix notation of Ref. 19, if $M = 2N$ and L poles are known, then we solve the equation

$$AB = C \qquad (C.7)$$

where A is a square matrix defined as

$$A = \begin{bmatrix} 1 & z_1 & z_1^2 & \cdots & z_1^{N-1} \\ 1 & z_2 & z_2^2 & \cdots & z_2^{N-1} \\ \vdots & \vdots & \vdots & & \vdots \\ 1 & z_L & z_L^2 & & z_L^{N-1} \\ I_0 & I_1 & I_2 & \cdots & I_{N-1} \\ I_1 & I_2 & I_3 & \cdots & I_N \\ \vdots & \vdots & \vdots & & \vdots \\ I_{N-1-L} & I_{N-L} & I_{N-L+1} & \cdots & I_{2N-L-2} \end{bmatrix} \qquad (C.8a)$$

and B and C are vectors defined as

$$B = \begin{bmatrix} \alpha_0 \\ \alpha_1 \\ \vdots \\ \alpha_{N-1} \end{bmatrix} \qquad (C.8b) \qquad\qquad C = - \begin{bmatrix} z_1^N \\ z_2^N \\ \vdots \\ z_L^N \\ I_N \\ I_{N+1} \\ \vdots \\ I_{2N-1-L} \end{bmatrix} \qquad (C.8c)$$

If $M > 2N$ and L poles are known, then the solution takes on a pseudo-inverse or least-squares form as

$$A^T A B = A^T C \qquad (C.9)$$

where A^T is the transpose of the matrix A and A is now a rectangular matrix of the form

$$A = \begin{bmatrix}
1 & z_1 & z_1^2 & \cdots z_1^{N-1} \\
1 & z_2 & z_2^2 & \cdots z_2^{N-1} \\
\vdots & \vdots & \vdots & \vdots \\
1 & z_L & z_L^2 & \cdots z_L^{N-1} \\
I_0 & I_1 & I_2 & \cdots I_{N-1} \\
I_1 & I_2 & I_3 & \cdots I_N \\
\vdots & \vdots & & \\
I^{M-N-1-L} & I_{M-N-L} & & \cdots I_{M-L-2}
\end{bmatrix} \qquad (C.10a)$$

$$B = \begin{bmatrix}
\alpha_0 \\
\alpha_1 \\
\alpha_2 \\
\vdots \\
\alpha_{N-1}
\end{bmatrix} \qquad (C.10b)$$

$$C = - \begin{bmatrix}
z_1^N \\
z_2^N \\
\vdots \\
z_L^N \\
I_N \\
\vdots \\
I_{M-1-L}
\end{bmatrix} \qquad (C.10c)$$

DATE
FILMED

0-8